Electronic Supplementary Information

Water-Soluble NHC Pd/Ni Bimetallic Nanoparticles for H/D Exchange in Aromatic Amino-Acids

Oscar Suárez-Riaño,[1] Gabriel Mencia,[2] Simon Tricard,[2] Jerome Esvan,[3] Pier-Francesco Fazzini,[2] Bruno Chaudret,[2] and Edwin A. Baquero[1]**

[1]*Estado Sólido y Catálisis Ambiental (ESCA), Departamento de Química, Facultad de Ciencias, Universidad Nacional de Colombia, Carrera 30 No. 45-03, 111321, Bogotá, Colombia.*

[2]*LPCNO, Laboratoire de Physique et Chimie de Nano-Objets, UMR, 5215 INSA-CNRS-UPS, Institut National des Sciences Appliques 135, Avenue de Rangueil, 31077, Toulouse, France.*

[3]*Institut Carnot – Centre Inter-universitaire de Recherche et d'Ingénierie des Matériaux, INP-ENSIACET, CNRS, Université de Toulouse, 118 Route de Narbonne, 31062, Toulouse, France*

E-mail: menciabe@insa-toulouse.fr (G.M.), eabaquerov@unal.edu.co (E.A.B.)

TABLE OF CONTENTS

1. General procedures and characterization techniques

Reagents

$Pd_2(dba)_3$ precursor was purchased from Nanomeps Toulouse, $Ni(COD)_2$ from Alfa-Aesar, L-phenylalanine, L-tyrosine, and L-histidine from Sigma-Aldrich, tetrahydrofuran from CARLO ERBA, D_2 and CO gas from Air liquid (France), ^{13}CO gas from Eurisotop, H_2 from Hydrogen Gas Generator AVANTEC model 40H (water electrolysis). All the reagents were used without further purification.

Transmission Electron Microscopy (TEM)

MNPs were observed by TEM after the deposition of a drop of a solution of the isolated NPs suspended in water over a copper grid coated with amorphous carbon. TEM analyses were performed at Raimond Castaing Microanalysis Centre (UAR 3623) (Toulouse, France) using a JEOL JEM 1400 electron microscope working at 120 kV. The NPs average size approximation was made by manual analysis of the magnified micrographs measuring 200 particles on a given grid using ImageJ software.

High Resolution TEM coupled to Energy Dispersive X-ray Spectroscopy (HR-TEM-EDX)

MNPs were observed by HR-TEM after the deposition of a drop of a solution of the isolated MNPs suspended in THF or water over a holey carbon-coated copper grid. HR-TEM analysis was performed at Raimond Castaing Microanalysis Centre (UAR 3623) (Toulouse, France). TEM and scanning transmission electron microscopy (STEM) studies were performed using a JEOL cold-FEG JEM-ARM200F operated at 200kV equipped with a probe Cs corrector reaching a spatial resolution of 0.078 nm. EDX spectra were recorded on a JEOL CENTURIO SDD detector.

Thermogravimetric analysis (TGA)

TGA analyses were performed in a TGA/DSC 1 STAR System equipped with an ultra-microbalance UMX5, a gas switch GC200 and sensors DTA and DSC. The samples were analyzed through a two steps oxidation/reduction method. First the sample was heated from 25 °C to 500 °C at 20°C/min under air and kept at 500 ºC during 2h. After cooling down, it was heated again from 25 °C to 700 °C at 30 °C/min under a gas mixture Ar/H_2 4% and kept at 700 ºC during 3h.

Attenuated Total Reflection Fourier Transform Infrared Spectroscopy (ATR-FTIR)

ATR-FTIR spectra were recorded using a Thermo Scientific Nicolet 6700 spectrophotometer using Ge tip in the range of 4000-600 cm^{-1}

Nuclear Magnetic Resonance (NMR)

^1H and ^{13}C NMR experiments were recorded in a 500 MHz Bruker Avance spectrometer using deuterated solvents with internal or external TMS reference.

Solid-State Nuclear Magnetic Resonance (SS-NMR)

Solid-state NMR experiments were recorded at the Laboratoire de Chimie de Coordination (Toulouse, France) on a Bruker Avance 400 spectrometer equipped with 3.2 mm probes. Samples were spun at 10.3 and 50 kHz at the magic angle using ZrO_2 rotors.

X-ray Photoelectron Spectroscopy (XPS)

XPS analysis were performed at CIRIMAT Laboratory (Toulouse) using a Thermoelectron Kalpha device. The photoelectron emission spectra were recorded using Al-Kα radiation (hν =1486.6 eV) from a monochromatized source. The analyzed area was about 0.15 mm^2. The pass energy was fixed at 40 eV. The spectrometer energy calibration was made using the C1s (284.5 ± 0.1 eV) photoelectron lines. XPS spectra were recorded in direct mode N(Ec). The background signal was removed using the Shirley method. The atomic concentrations were determined from photoelectron peak areas using the atomic sensitivity factors reported by Scofield,[1] taking into account the transmission function of the analyzer. The photoelectron peaks were analyzed by Gaussian/Lorentzian (G/L = 50) peak fitting.

Catalytic assay

Catalytic assays were carried out using L-phenylalanine, L-tyrosine, and L-histidine as substrates. Thus, 0.1399 mmol of the substrate, 2 mL of D_2O, and 4 mol% PdNi (**PdNi@IMesPrSO$_3$)**, 5 mol % Pd and Ni (**Pd@IMesPrSO$_3$** and **Ni@IMesPrSO$_3$**) (based on TGA, and ICP-MS analysis of the nanocatalysts), were added to a Fischer-Porter reactor. 2 bar of D_2 were added and the reaction was stirred at 55 ºC during 48 h. Then, an aliquot of the reaction was taken for NMR analysis. The deuteration percentage was calculated from the relationship between the integrals from the starting substrate and product.

2. Synthesis and characterization data for imidazolium salt and free carbene

Imidazolium salt (**IMesPrSO$_3$H**) was synthesized according to the method described by Shaugnessy and co-workers (Scheme S1).[2]

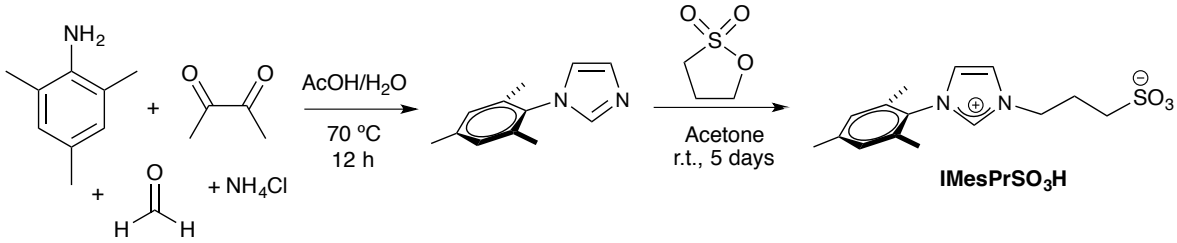

Scheme S1. Synthesis of imidazolium salt **IMesPrSO$_3$H**.

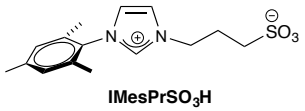

IMesPrSO$_3$H: glacial acetic acid (1.7 mL), formaldehyde (37 % aqueous solution, 0.19 g, 0.5 mL, 6.45 mmol) and glyoxal (40 % aqueous solution, 0.33 g, 0.8 mL, 7.18 mmol) were added with constant stirring at rt in a two-necked round-bottom flask. Subsequently, ammonium acetate (0.31 g, 4.04 mmol), glacial acetic acid (1.7 mL) and water were mixed in a vial, to which 2,4,6-trimethylaniline (81.1 mg, 0.08 mL, 0.60 mmol) was added. The solution containing the aniline was added dropwise into the two-necked round-bottom flask,

previously heated to 70 ºC. Then, it was stirred at 70 ºC for 20 hours and allowed to cool to room temperature (r. t.). The solution obtained was added to a saturated $NaHCO_3$ solution, allowing neutralization, and stirred for 1 hour at r. t. Subsequently, the solution was transferred to a Schlenck flask and dried under vacuum. To form the propylsulfonate chain, mesitylimidazole (1.27 g, 6.67 mmol) was added to acetone and propanesultone in excess (2.09 g, 17.1 mmol) and left to stir at r. t. for 5 days. **IMesPrSO$_3$H** was obtained as a white solid which is filtered and washed with acetone (0.14 g, 75%). (^{1}H-NMR dmso-d_6, 500 MHz): δ = 9.37 (t, $^4J_{H,H}$= 1.7 Hz, 1H, CH^2 Im), 8.11 (t, $^4J_{H,H}$= 1.8 Hz, 1H, CH^5 Im), 7.92 (t, $^4J_{H,H}$= 1.8 Hz, 1H, CH^4 Im), 7.14 (s, 2H, *m*-CH IMes), 4.42 (t, $^3J_{H,H}$= 7.2 Hz, 2H, $CH_2CH_2CH_2$), 2.44 (t, $^3J_{H,H}$= 7.1 Hz, 2H, $CH_2CH_2CH_2$), 2.33 (s, 3H, *p*-CH_3 IMes), 2.20 (quint, $^3J_{H,H}$= 7.2 Hz, 2H, $CH_2CH_2CH_2$), 2.02 (s, 6H, *o*-CH_3 IMes) ppm. (Figure S20).

IMesPrSO$_3$: free carbene was synthesized before used it as stabilizer for Pd and Ni NPs, and their ^{1}H NMR spectrum were recorded *in situ*. The free carbene was formed by the addition of potassium *tert*-butoxide (1.2 eq) to the imidazolium salt (1 eq) solution in THF and allowed to react for 7 hours.

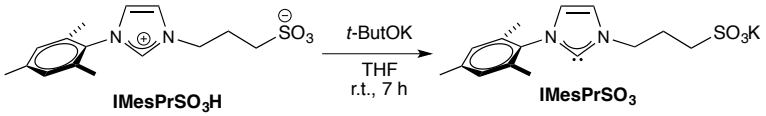

Scheme S2. Synthesis of **IMesPrSO$_3$**.

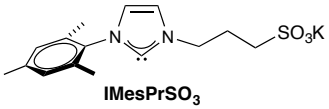

IMesPrSO$_3$: 0.0242 g (0.0785 mmol) of **IMesPrSO$_3$H** and 0.0108 g (0.0962 mmol) of potassium *tert*-butoxide were added in a Schlenck tube with 5 mL of THF and allowed to react for 7 h (Scheme S2). Afterwards, the solution was evaporated under vacuum and re-dissolved in $CDCl_3$ under inert atmosphere and the ^{1}H NMR spectrum was recorded immediately. (^{1}H-NMR dmso-d_6, 500 MHz): 7.73 (d, $^2J_{H,H}$= 2.01 Hz, 1H, CH^5 Im), 7.50 (d, $^2J_{H,H}$= 2.05 Hz, 1H, CH^4 Im), 7.07 (s, 2H, *m*-CH IMes), 4.43 (t, $^3J_{H,H}$= 7.2 Hz, 2H, $CH_2CH_2CH_2$), 2.88 (t, $^3J_{H,H}$= 7.1 Hz, 2H, $CH_2CH_2CH_2$), 2.34 (quint, $^3J_{H,H}$= 7.2 Hz, 2H, $CH_2CH_2CH_2$), 2.26 (s, 3H, *p*-CH_3 IMes), 1.96 (s, 6H, *o*-CH_3 IMes) ppm. (Figure S21)

3. Synthesis and characterization data for Pd, Ni and PdNi nanoparticles

All the nanoparticles synthesis were carried out inside the glove box and under inert atmosphere. Palladium nanoparticles were synthesized using the procedure designed by Chaudret and co-workers known as the organometallic approach.[3]

Pd, Ni, and PdNi nanoparticles were synthesized by the addition of the stabilizer (**IMesPrSO$_3$**).

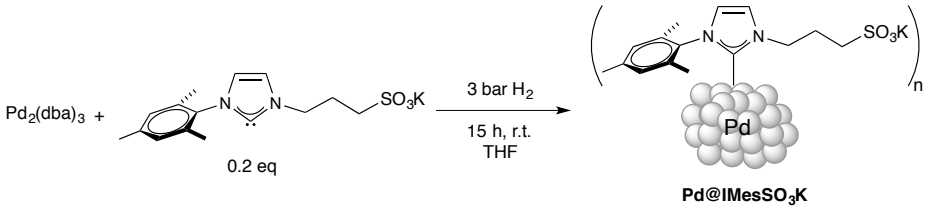

Scheme S3. Synthesis of **Pd@IMesPrSO$_3$**.

Pd@IMesPrSO$_3$: IMesPrSO$_3$ was synthesized before used it as stabilizer, as it was already mentioned (Scheme S2). The free carbene was formed by the addition of potassium *tert*-butoxide (20 mol% excess) to the imidazolium salt solution in THF and allowed to react for 7 hours. This solution was filtered through Celite® to remove the salt excess. 0.183 g (0.1998 mmol) of $Pd_2(dba)_3$ were added to a Fischer-Porter with THF (15 mL) under inert atmosphere. Subsequently, the filtered free carbene solution was added (0.2 eq). To this solution, 3 bar of H_2 were added and allowed to react at r. t. overnight (Scheme S3). Finally, the PdNPs were precipitated and washed with pentane (3 x 30 mL) and dried under vacuum overnight.

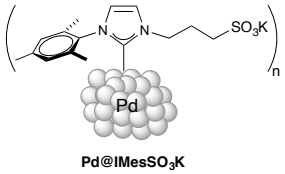

Pd@IMesSO$_3$K

Pd@IMesPrSO$_3$: 0.0247 g (0.0800 mmol) of **IMesPrSO$_3$H** and 0.0108 g (0.0962 mmol) of potassium *tert*-butoxide were used, along with 0.183 g (0.1998 mmol) of $Pd_2(dba)_3$ with the method above described (78.3 % yield based on Pd determine by TGA). **Pd:NHC ratio:** 5:1. **TEM:** 2.1 ± 0.3 nm. **HRTEM**: fcc Pd nanoparticles.

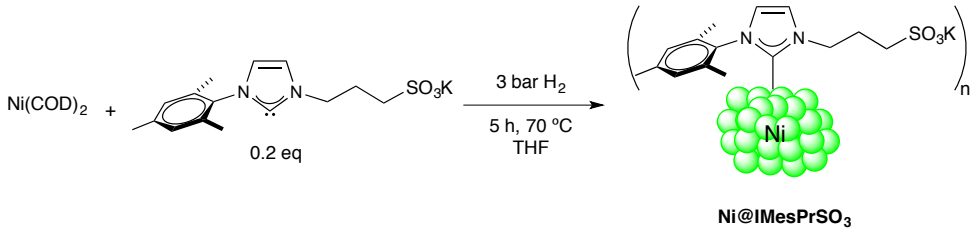

Ni@IMesPrSO$_3$

Scheme S4. Synthesis of **Ni@IMesPrSO$_3$**.

Ni@IMesPrSO$_3$: IMesPrSO$_3$ was synthesized before used it as stabilizer, as it was already mentioned (Scheme S2). The free carbene was formed by the addition of potassium *tert*-butoxide (1.2 eq) to the imidazolium salt (1 eq) solution in THF and allowed to react for 7 hours. This solution was filtered through Celite® to remove the salt excess. 0.1100 g (0.400 mmol) of $Ni(COD)_2$ were added to a Fischer-Porter with THF (15 mL) under inert atmosphere. Subsequently, the filtered free carbene solution was added (0.2 eq). To this solution, 3 bar of H_2 were added and allowed to react at 70 ºC during 5 h (Scheme S4). Finally, the NiNPs were precipitated and washed with pentane (3 x 30 mL) and dried under vacuum overnight.

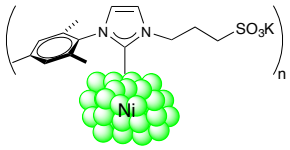

Ni@IMesPrSO$_3$

Ni@IMesPrSO$_3$: 0.0247 g (0.0800 mmol) of **IMesPrSO$_3$H** and 0.0108 g (0.0962 mmol) of potassium *tert*-butoxide were used, along with 0.1100 g (0.400 mmol) of $Ni(COD)_2$ with the method above described (90.5 % yield based on Ni determine by TGA). **Pd:NHC ratio:** 5:1. **TEM:** 1.8 ± 0.4 nm.

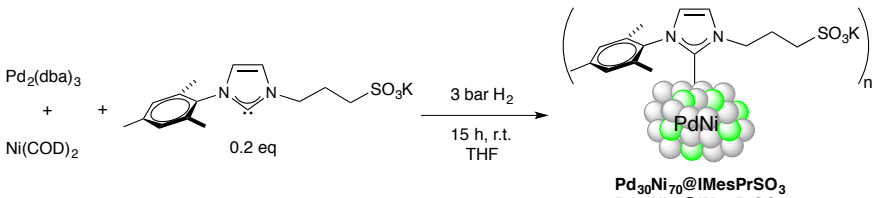

Pd$_{30}$Ni$_{70}$@IMesPrSO$_3$
Pd$_{50}$Ni$_{50}$@IMesPrSO$_3$
Pd$_{70}$Ni$_{30}$@IMesPrSO$_3$

Scheme S5. Synthesis of bimetallic **PdNi@IMesPrSO$_3$** NPs.

PdNi@IMesPrSO$_3$ (Scheme S5): **IMesPrSO$_3$** was synthesized before used it as stabilizer, as it was already mentioned (Scheme S2). The free carbene was formed by the addition of potassium *tert*-butoxide (1.2 eq) to the imidazolium salt (1 eq) solution in THF and allowed to react for 7 hours. This solution was filtered through Celite® to remove the salt excess. $Pd_2(dba)_3$ and $Ni(COD)_2$ in different molar percentages (30:70, 50:50, 70:30) were added to a Fischer-Porter under inert atmosphere with THF (15 mL) under inert atmosphere. Subsequently, the filtered free carbene solution was added (0.2 eq). To this solution, 3 bar of H_2 were added and allowed to react at r. t. overnight (Scheme S5). Finally, the PdNiNPs were precipitated and washed with pentane (3 x 30 mL) and dried under vacuum overnight.

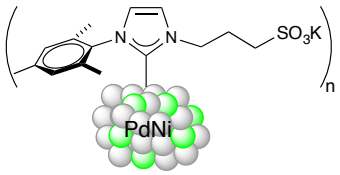

$Pd_{30}Ni_{70}$@IMesPrSO$_3$

$Pd_{30}Ni_{70}$@IMesPrSO$_3$: 0.0496 g (0.1600 mmol) of **IMesPrSO$_3$H** and 0.0215 g (0.192 mmol) of potassium *tert*-butoxide were used, along with 0.1098 g (0.120 mmol) of $Pd_2(dba)_3$ and 0.154 g (0.560 mmol) of $Ni(COD)_2$ with the method above described (65.9 % yield based on Pd and Ni based on ICP-MS). **Pd:Ni molar ratio:** 32:68, determined by ICP-MS. **TEM:** 2.5 ± 0.3 nm.

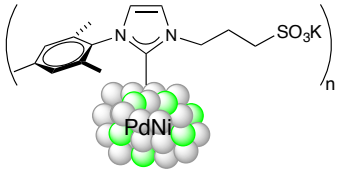

$Pd_{50}Ni_{50}$@IMesPrSO$_3$

$Pd_{50}Ni_{50}$@IMesPrSO$_3$: 0.0496 g (0.1600 mmol) of **IMesPrSO$_3$H** and 0.0215 g (0.192 mmol) of potassium *tert*-butoxide were used, along with 0.183 g (0.1998 mmol) of $Pd_2(dba)_3$ and 0.1100 g (0.400 mmol) of $Ni(COD)_2$ with the method above described (70.2 % yield based on Pd and Ni based on ICP-MS). **Pd:Ni molar ratio:** 44:55, determined by ICP-MS. **TEM:** 2.9 ± 0.4 nm.

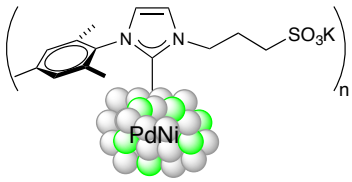

$Pd_{70}Ni_{30}$@IMesPrSO$_3$

$Pd_{70}Ni_{30}$@IMesPrSO$_3$: 0.0496 g (0.1600 mmol) of **IMesPrSO$_3$H** and 0.0215 g (0.192 mmol) of potassium *tert*-butoxide were used, along with 0.256 g (0.280 mmol) of $Pd_2(dba)_3$ and 0.0660 g (0.240 mmol) of $Ni(COD)_2$ with the method above described (77.2 % yield based on Pd and Ni based on ICP-MS). **Pd:Ni molar ratio:** 63:37, determine by ICP-MS. **TEM:** 2.5 ± 0.3 nm. **HRTEM**: cubic PdNi bimetallic nanoparticles

4. ICP-MS determination

Table S1. Mass and molar percentages of Pd and Ni in bimetallic NPs determined by ICP-AES.

Entry	MNPs	Ni ppm	Pd ppm	Mass (mg)	Vol (mL)	Ni % mass	Pd % mass	Pd:Ni ratio
1	$Pd_{30}Ni_{70}$@IMesPrSO$_3$	36.09	30.79	9.98	50	18.08	15.43	32:68
2		36.26	30.76	9.98	50	18.17	15.41	
3	$Pd_{50}Ni_{50}$@IMesPrSO$_3$	29.41	41.95	9.46	50	15.54	22.17	45:55
4		29.60	43.09	9.46	50	15.65	22.78	
5	$Pd_{70}Ni_{30}$@IMesPrSO$_3$	19.32	58.71	8.91	50	10.84	32.95	63:37
6		19.53	58.97	8.91	50	10.96	33.09	

5. XRD measuraments for PdNPs, NiNPs and PdNiNPs

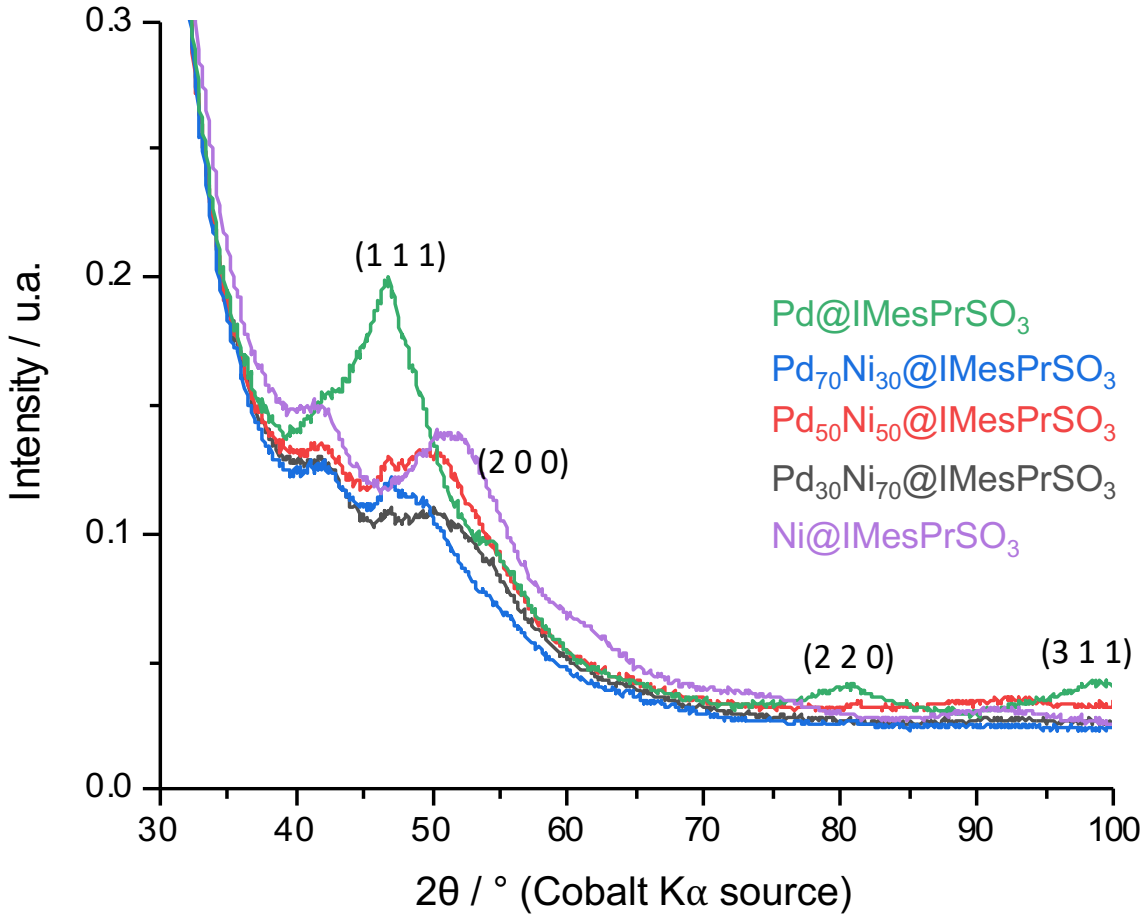

Figure S1. XRD diffractogram for **MNPs**.

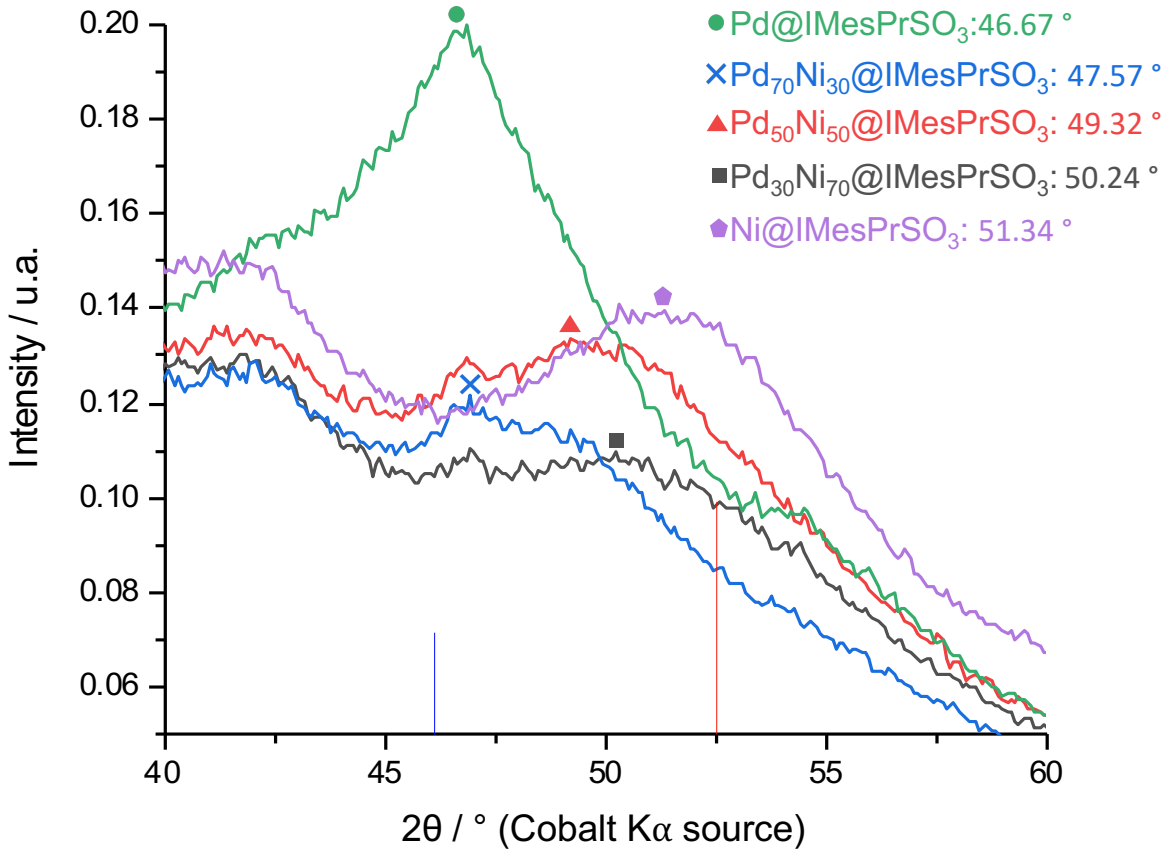

Figure S2. XRD diffractogram for **MNPs** in (111) plane.

Table S2. Diffraction angle (2θ) values of the 111 lattice of **MNPs**.

Entry	MNPs	2θ for (111) (°)
1	**$Pd@IMesPrSO_3$**	46.67
2	**$Pd_{70}Ni_{30}@IMesPrSO_3$**	47.57
3	**$Pd_{50}Ni_{50}@IMesPrSO_3$**	49.32
4	**$Pd_{30}Ni_{70}@IMesPrSO_3$**	50.24
5	**$Ni@IMesPrSO_3$**	51.34

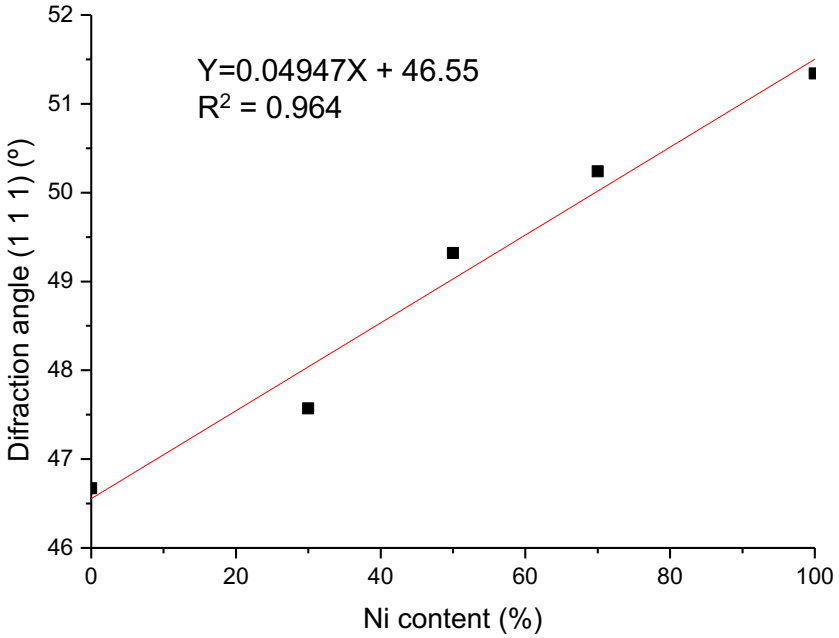

Figure S3. Linear fitting of the relationship between diffraction angle value and Pd:Ni ratio in **MNPs**.

6. TEM images for PdNPs, NiNPs and PdNi

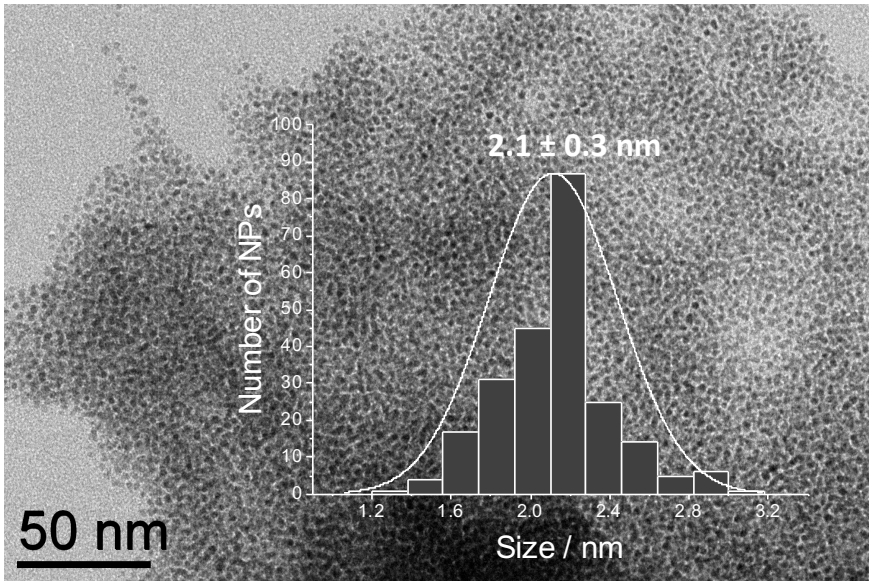

Figure S4. TEM micrograph and size distribution for **Pd@IMesPrSO$_3$** NPs.

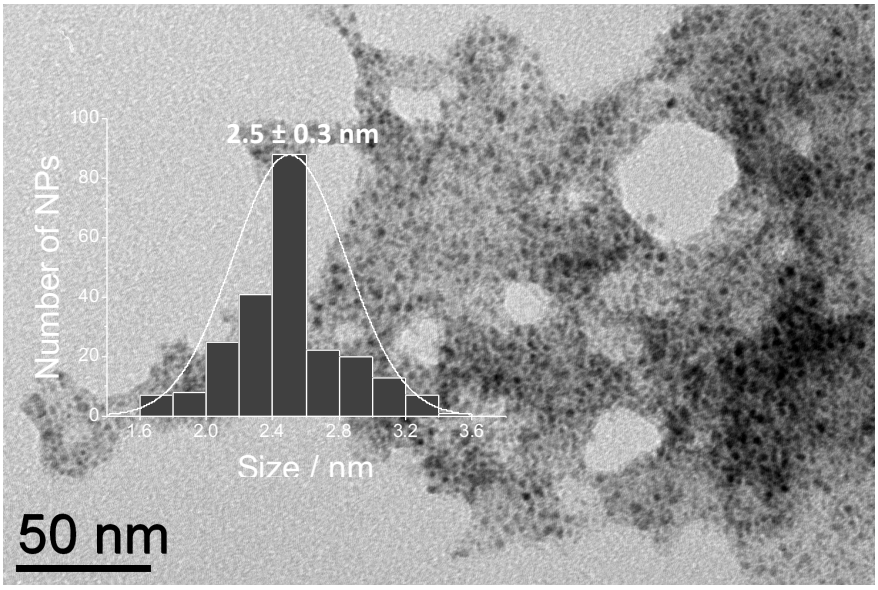

Figure S5. TEM micrograph and size distribution for **Pd$_{30}$Ni$_{70}$@IMesPrSO$_3$** NPs.

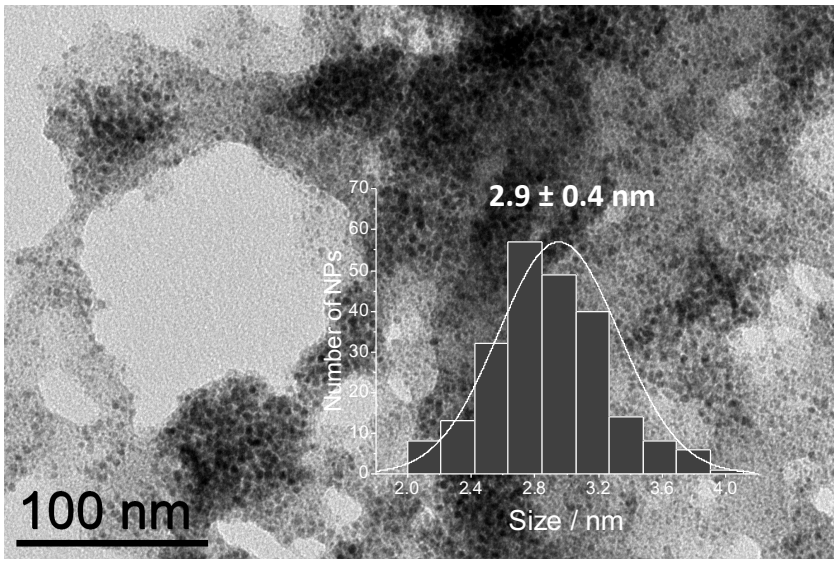

Figure S6. TEM micrograph for **$Pd_{50}Ni_{50}$@IMesPrSO$_3$** NPs.

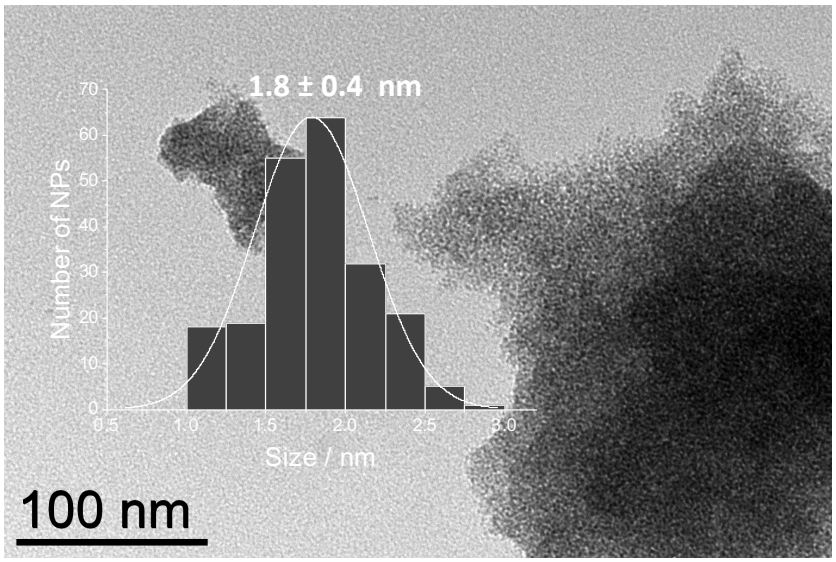

Figure S7. TEM micrograph for **Ni@IMesPrSO$_3$** NPs.

Table S3. Sizes of NPs obtained.

Entry	MNPs	Size (nm)
1	**Pd@IMesPrSO$_3$**	2.1 ± 0.3
2	**$Pd_{30}Ni_{70}$@IMesPrSO$_3$**	2.5 ± 0.3
3	**$Pd_{50}Ni_{50}$@IMesPrSO$_3$**	2.9 ± 0.4
4	**$Pd_{70}Ni_{30}$@IMesPrSO$_3$**	2.6 ± 0.3
5	**Ni@IMesPrSO$_3$**	1.8 ± 0.4

7. HR-TEM images for Pd and PdNi NPs

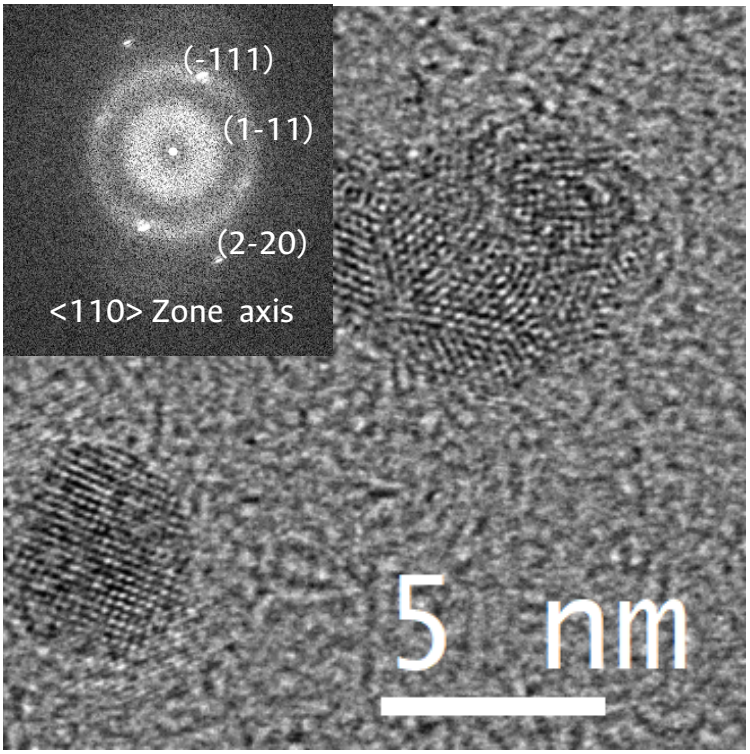

Figure S8. HR-TEM micrograph and FFT analysis (inset) for **Pd@IMesPrSO$_3$** NPs.

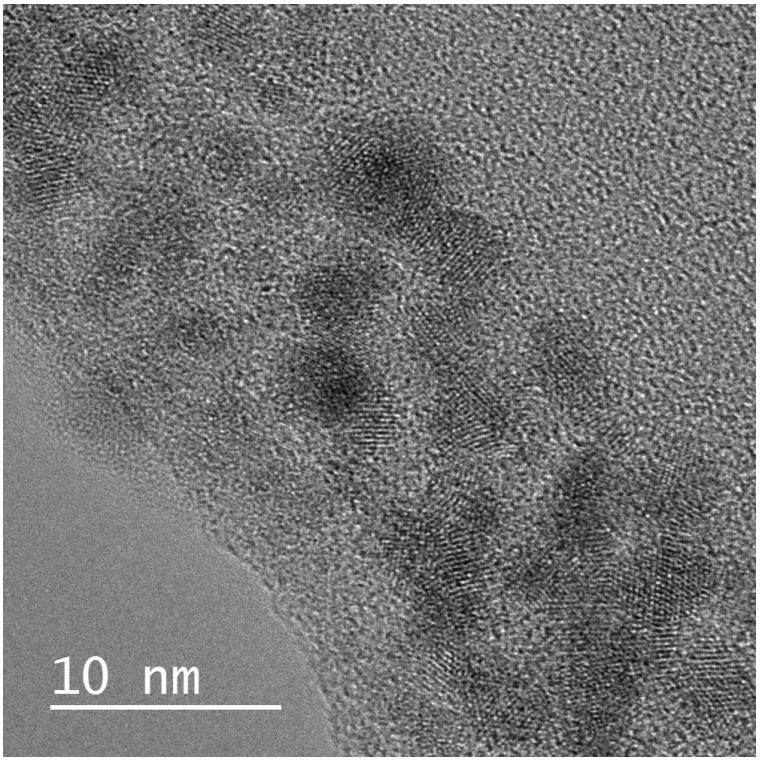

Figure S9. HR-TEM micrograph for **Pd$_{50}$Ni$_{50}$@IMesPrSO$_3$** NPs.

8. EDX spectra for Pd and PdNi NPs

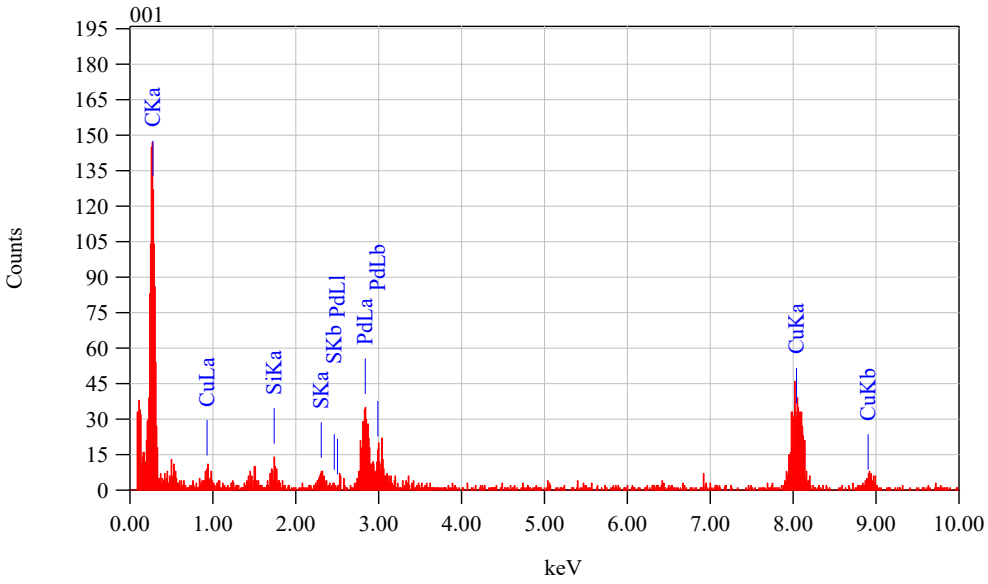

Figure S10. EDX spectrum for **Pd@IMesPrSO$_3$** NPs

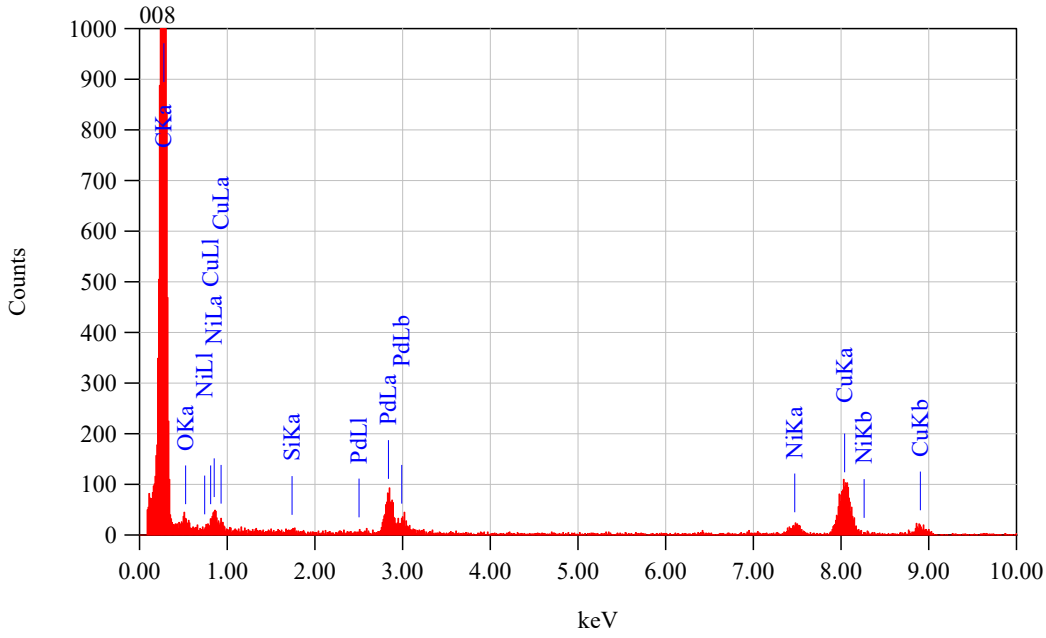

Figure S11. EDX spectrum for **Pd$_{70}$Ni$_{30}$@IMesPrSO$_3$** NPs (71.89 Pd %, 28.11 Ni %).

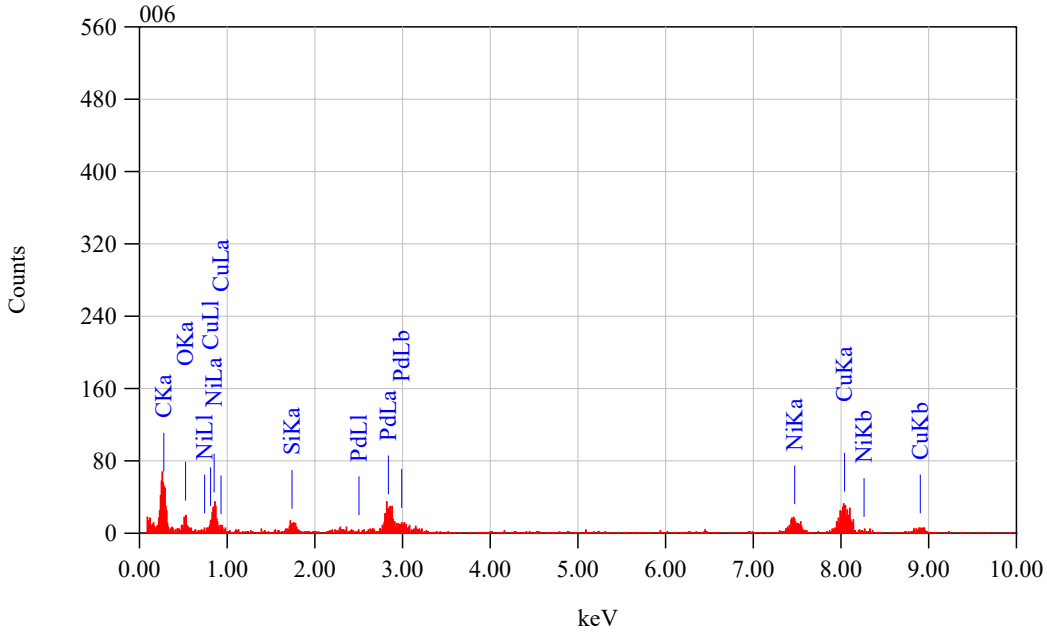

Figure S12. EDX spectrum for **$Pd_{50}Ni_{50}$@IMesPrSO$_3$** NPs (57.89 Pd %, 42.11 Ni %).

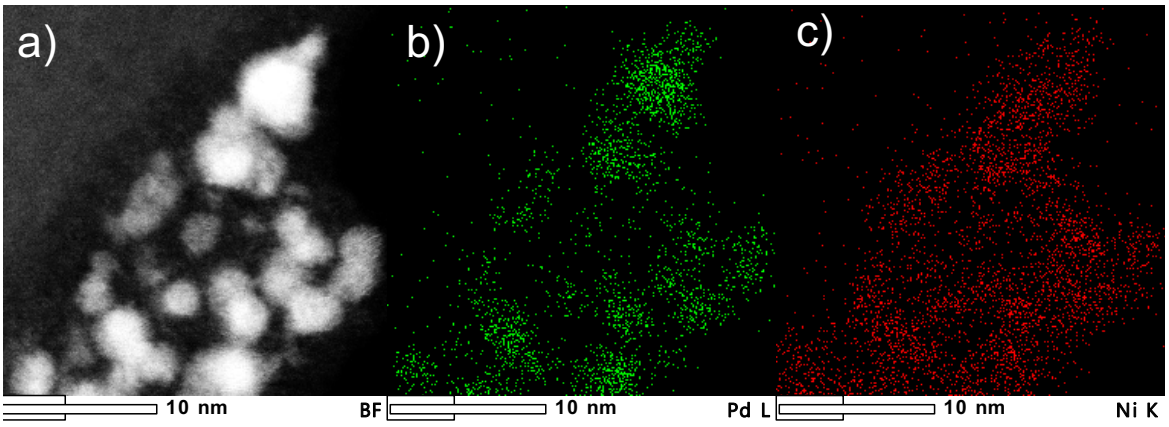

Figure S13. a) HR-STEM-HAADF image of **$Pd_{50}Ni_{50}$@IMesPrSO$_3$** NPs, and (b-c) Elemental mapping.

9. IR spectra

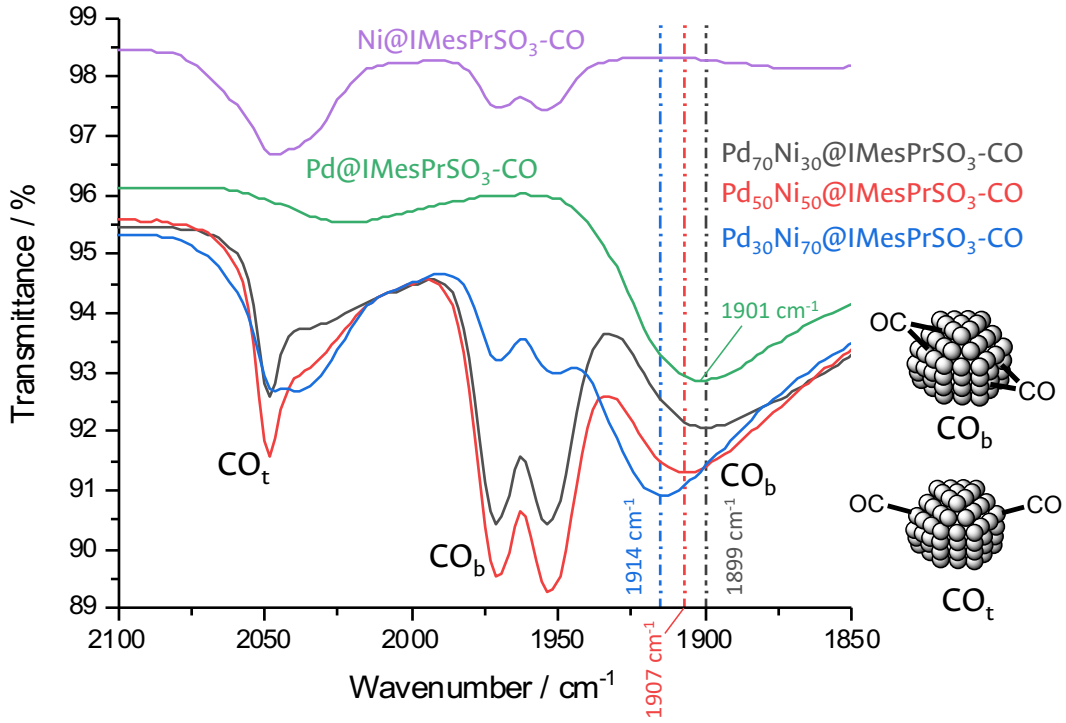

Figure S14. ATR-FTIR spectra for **Pd@IMesPrSO₃** (green), **Ni@IMesPrSO₃** (purple), **$Pd_{30}Ni_{70}$@IMesPrSO₃** (black), **$Pd_{50}Ni_{50}$@IMesPrSO₃** (red), **$Pd_{70}Ni_{30}$@IMesPrSO₃** (blue) after exposure to CO.

Table S4. CO_b band wavenumber for MNPs.

Entry	MNPs	CO_b (cm^{-1})
1	**Pd@IMesPrSO₃**	1901
2	**$Pd_{70}Ni_{30}$@IMesPrSO₃**	1899
3	**$Pd_{50}Ni_{50}$@IMesPrSO₃**	1907
4	**$Pd_{30}Ni_{70}$@IMesPrSO₃**	1914
5	**Ni@IMesPrSO₃**	-

10. Solid-State NMR spectra

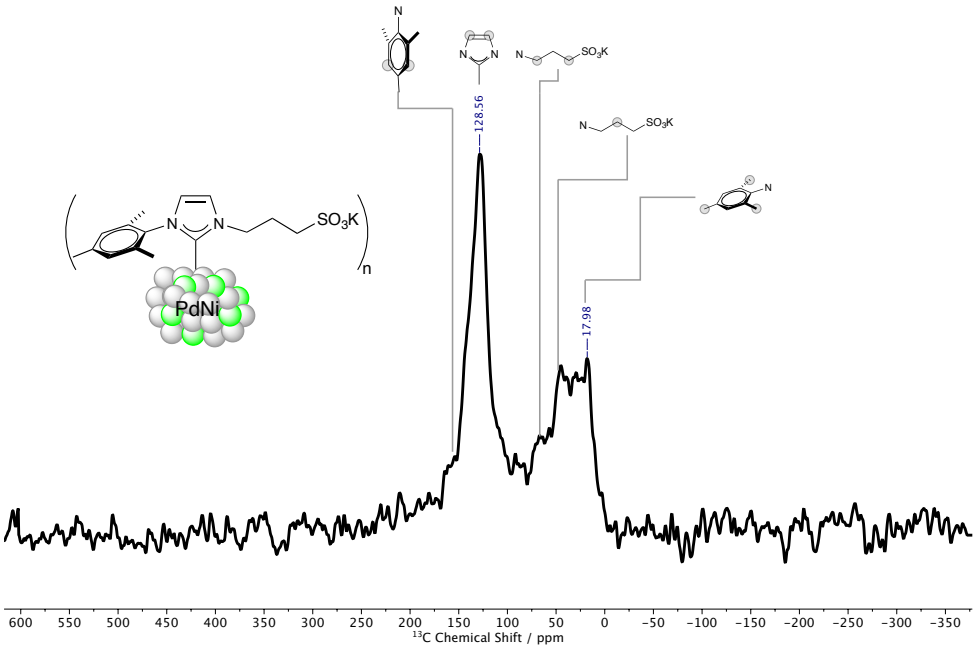

Figure S15. ^{13}C MAS Solid State NMR (100 MHz, spin at 50 kHz) spectrum for **$Pd_{70}Ni_{30}$@IMesPrSO$_3$**.

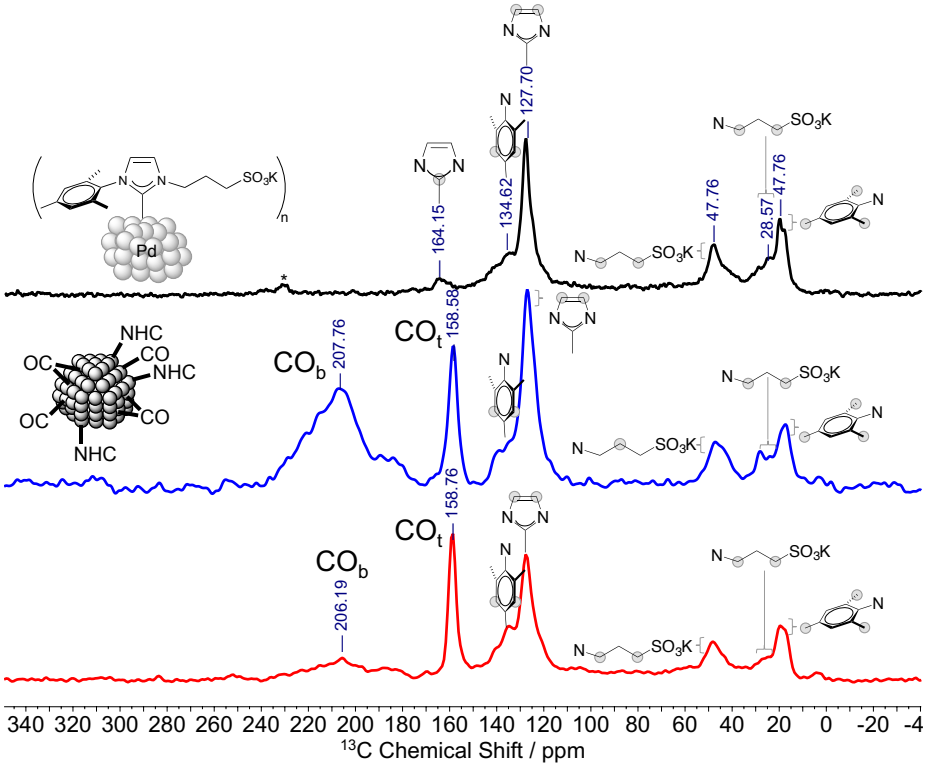

Figure S16. ^{1}H–^{13}C CP-MAS Solid State NMR (100 MHz, spin at 12.5 kHz) spectrum for **Pd@IMesPrSO$_3$** before exposure with ^{13}CO (black) (the peak denoted with an asterisk corresponds to a side spinning band),^{13}C MAS (blue) and ^{1}H–^{13}C CP-MAS (red) Solid State NMR (100 MHz, spin at 12.5 kHz) spectra for **Pd@IMesPrSO$_3$** after exposure to ^{13}CO.

11. XPS spectra

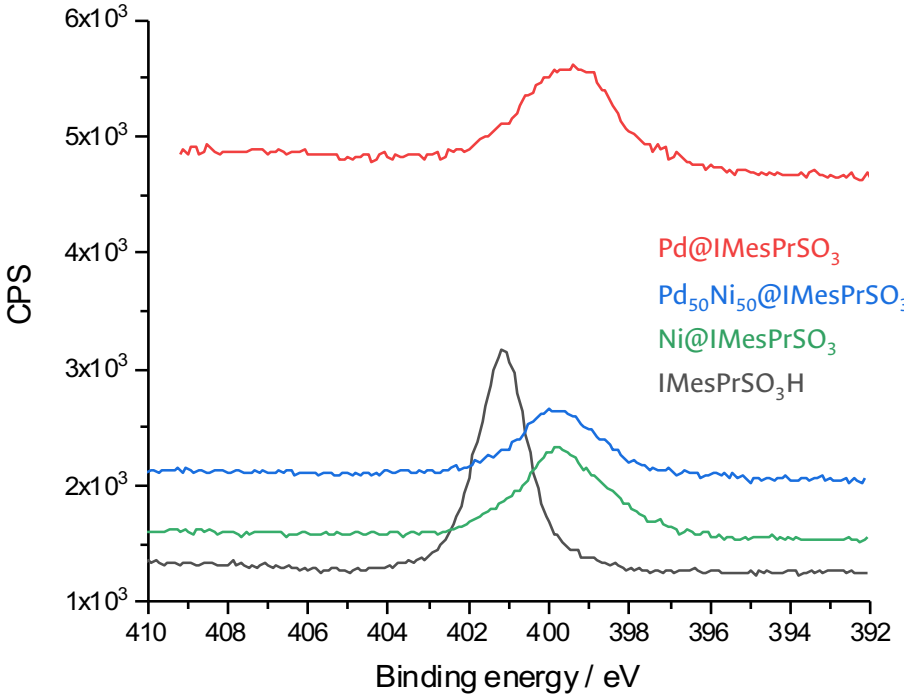

Figure S17. XPS spectra of the N1s signals for **IMesPrSO$_3$H** (black), **Pd@IMesPrSO$_3$** (red), **Pd$_{50}$Ni$_{50}$@IMesPrSO$_3$** (blue), and **Ni@IMesPrSO$_3$** (green).

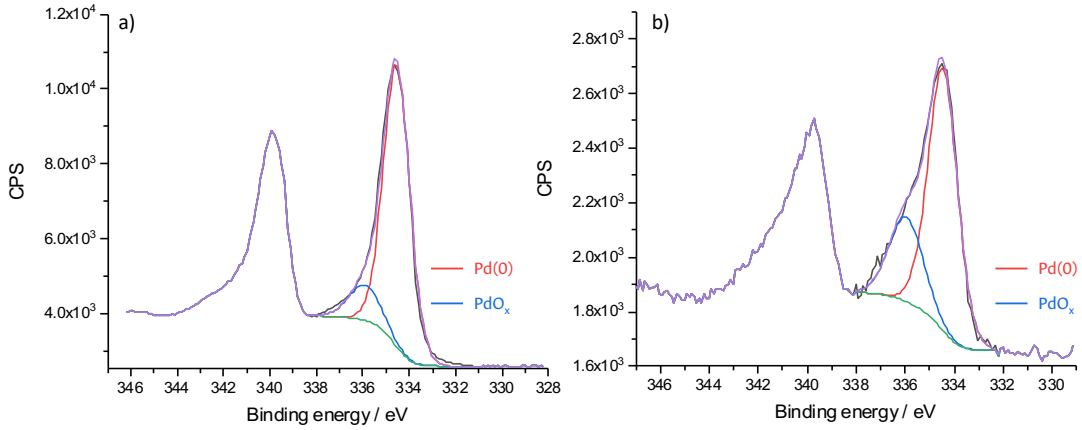

Figure S18. XPS spectra of the Pd3d 5/2 signals and deconvoluted signals for a) **Pd@IMesPrSO$_3$**, and b) **Pd$_{50}$Ni$_{50}$@IMesPrSO$_3$**.

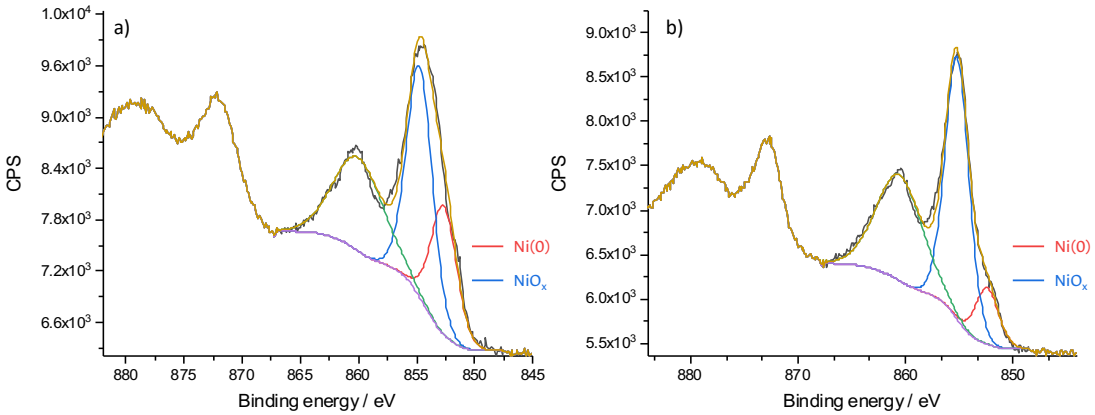

Figure S19. XPS spectra of the Ni2p 3/2 signals and deconvoluted signals for a) **Ni@IMesPrSO$_3$**, and b) **Pd$_{50}$Ni$_{50}$@IMesPrSO$_3$**.

X-ray Photoelectron Spectroscopy (XPS) has been presented as an alternative to observe the coordination mode of the stabilizing ligands on the metal surface.[4,5] Thus, XPS was performed on the samples **Pd@IMesPrSO$_3$**, **Pd$_{50}$Ni$_{50}$@IMesPrSO$_3$**, and **Ni@IMesPrSO$_3$**. By observing the change in the binding energy of the N1s signals from imidazolium salt **IMesPrSO$_3$H** (~ 401 eV), compared to **Pd@IMesPrSO$_3$**, **Pd$_{50}$Ni$_{50}$@IMesPrSO$_3$**, and **Ni@IMesPrSO$_3$** (~ 399 eV) (Figure S17), we can conclude that NPs are stabilized by NHC coordination and not by electrostatic interactions with the imidazolium salt.[4] This coordination, usually strong, explains the high colloidal stability in water observed for these NPs.[6]

Regarding Pd-based NPs, the Pd3d$_{5/2}$ spectra (Figure S18) can be deconvoluted in two components corresponding to metallic Pd (334 eV) and oxidized Pd (336 eV).[7] The latter can be attributed to the coordination of the NHC.[8] On another hand, regarding Ni-based NPs, the Ni2p$_{3/2}$ signals into three components, around 852 eV, 855 eV and 861 eV. These peaks are attributed to metallic Ni,[9] oxidized Ni,[10] and to satellite peaks, respectively (Figure S19). The presence of metal oxides in the samples is likely due to an oxidation in air during the transfer of the samples into the XPS machine.

12. NMR spectra

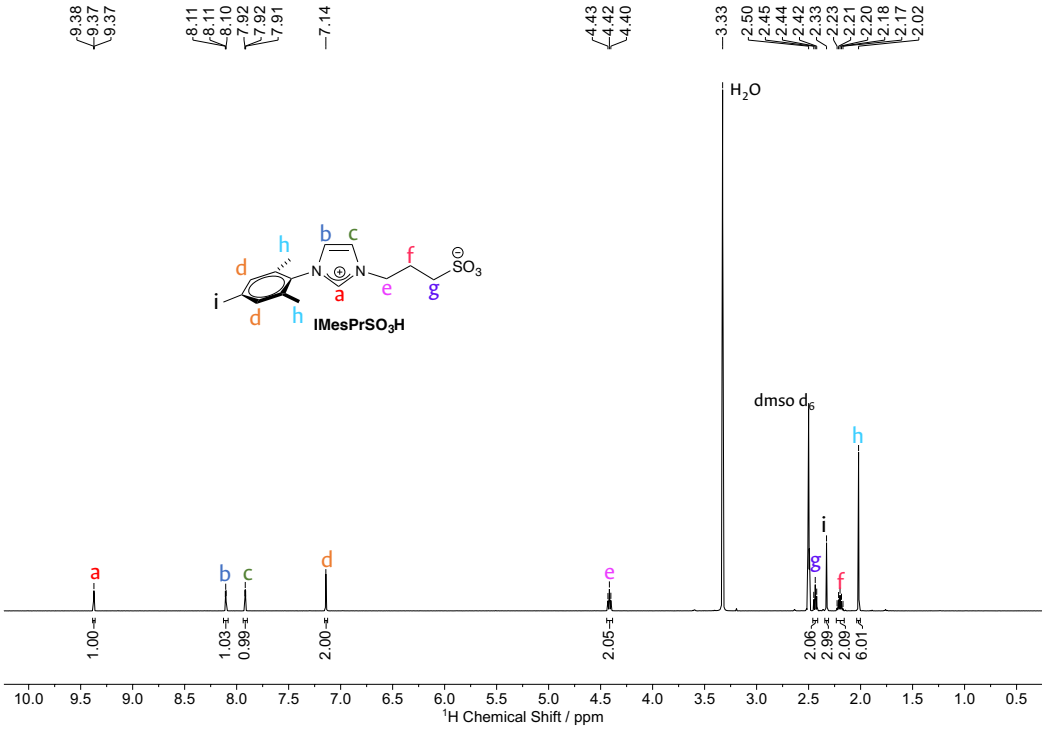

Figure S20. ^{1}H NMR (500 MHz, dmso-*d*$_6$) spectrum for **IMesPrSO$_3$H**.

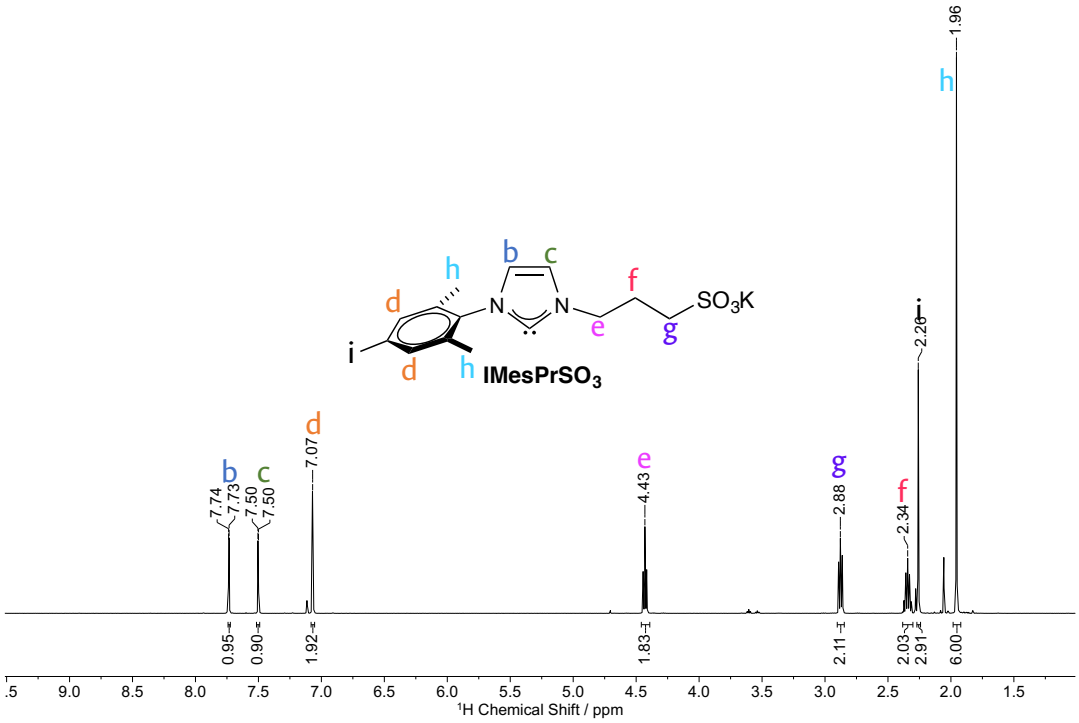

Figure S21. ^{1}H NMR spectrum (500 MHz, $CDCl_3$) for **IMesPrSO$_3$**.

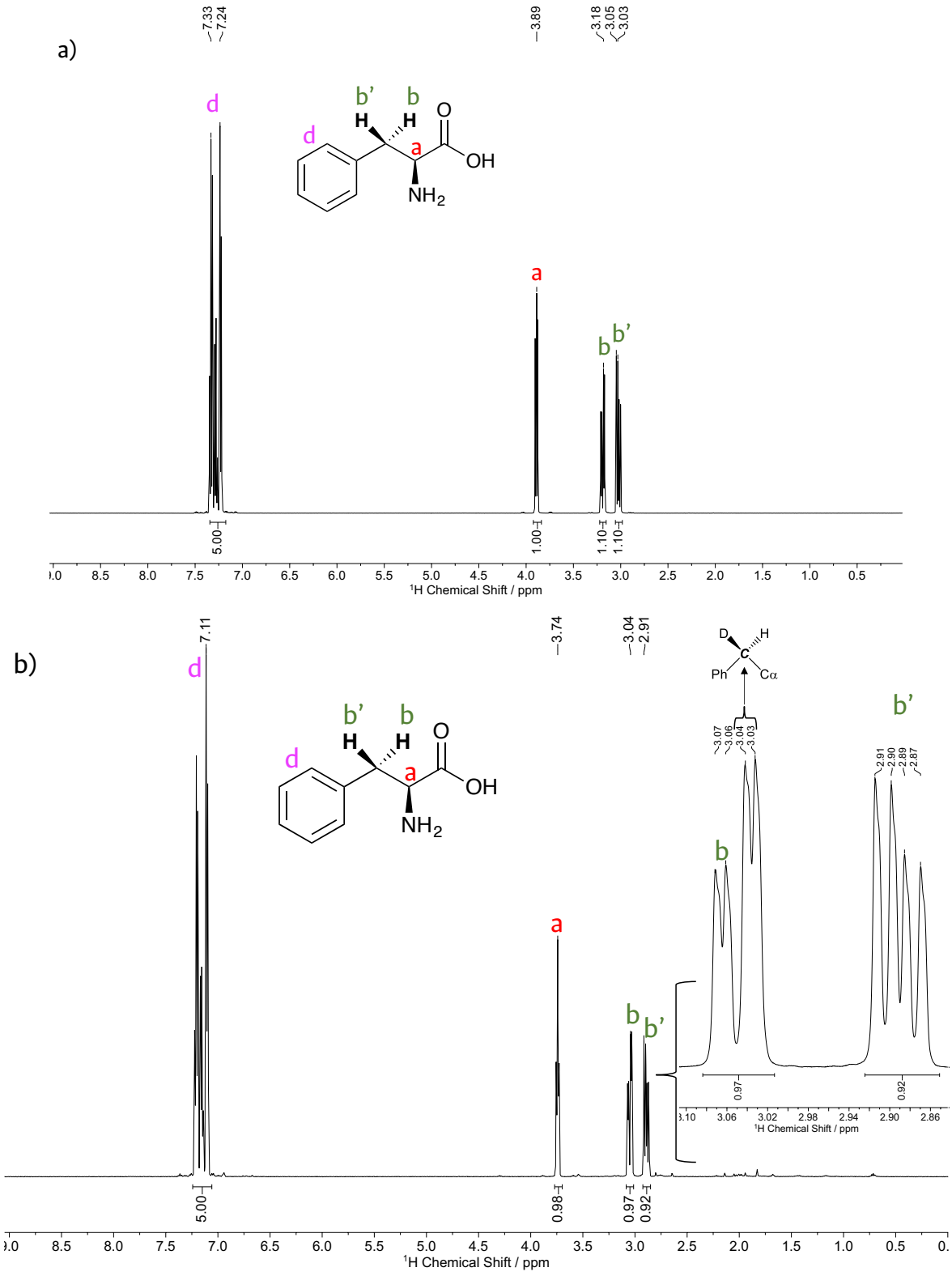

Figure S22. a) L-phenylalanine ^{1}H NMR spectrum before deuteration, b) L-phenylalanine deuteration using **Pd@IMesPrSO$_3$** (48 h, 55 ºC, 2 bar D_2, 5 mol % Pd) (Table 1, Entry 1).

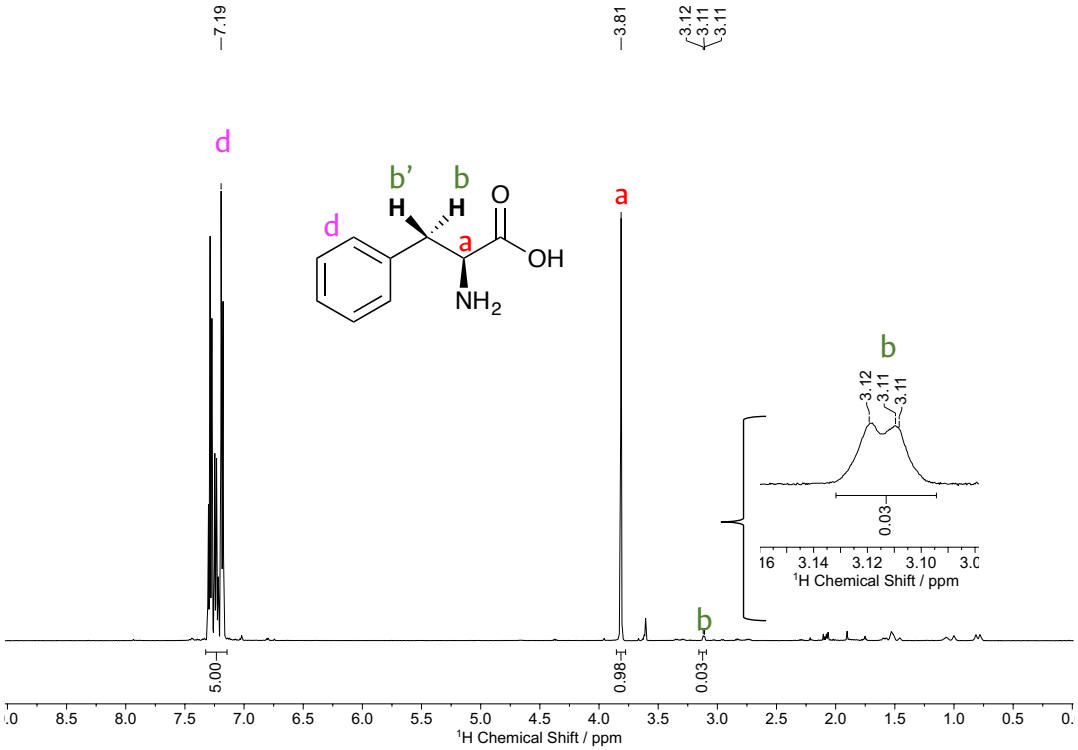

Figure S23. L-phenylalanine deuteration using **$Pd_{70}Ni_{30}$@IMesPrSO$_3$** (48 h, 55 ºC, 2 bar D_2, 4 mol % metal) (Table 1, Entry 2).

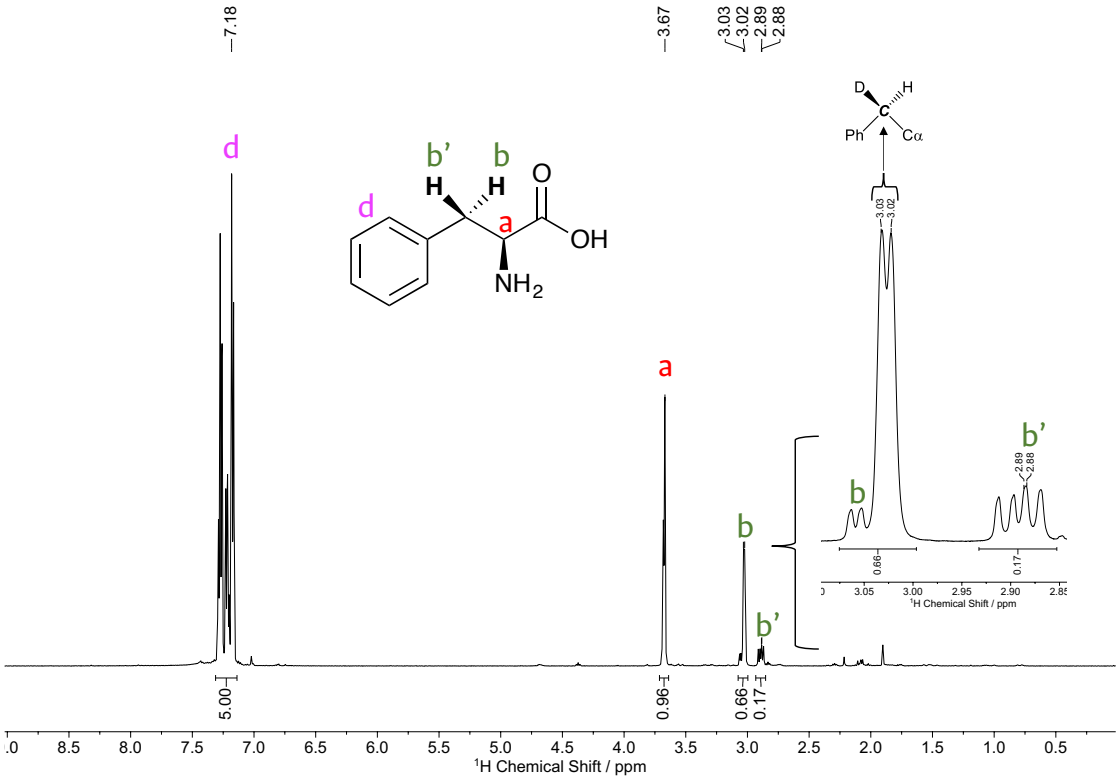

Figure S24. L-phenylalanine deuteration using **$Pd_{50}Ni_{50}$@IMesPrSO$_3$** (48 h, 55 ºC, 2 bar D_2, 4 mol % metal) (Table 1, Entry 3).

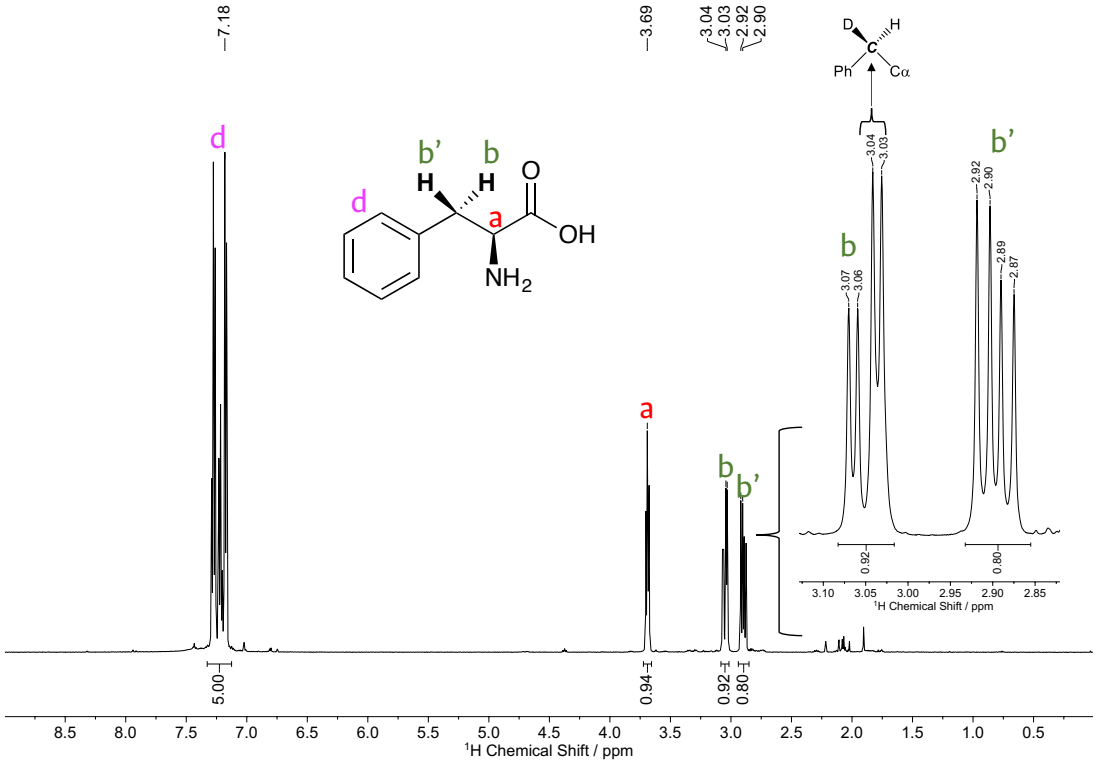

Figure S25. L-phenylalanine deuteration using **$Pd_{30}Ni_{70}$@IMesPrSO$_3$** (48 h, 55 ºC, 2 bar D_2, 4 mol % metal) (Table 1, Entry 4).

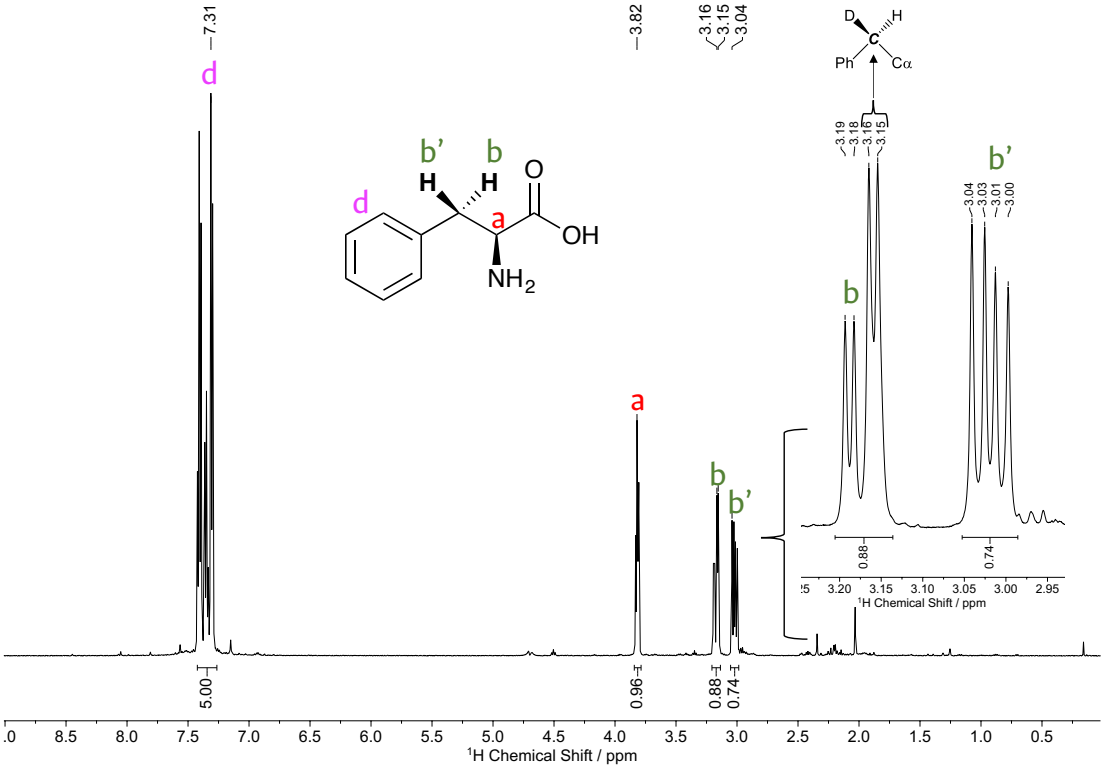

Figure S26. L-phenylalanine deuteration using **Ni@IMesPrSO$_3$** (48 h, 55 ºC, 2 bar D_2, 5 mol % Pd) (Table 1, Entry 5).

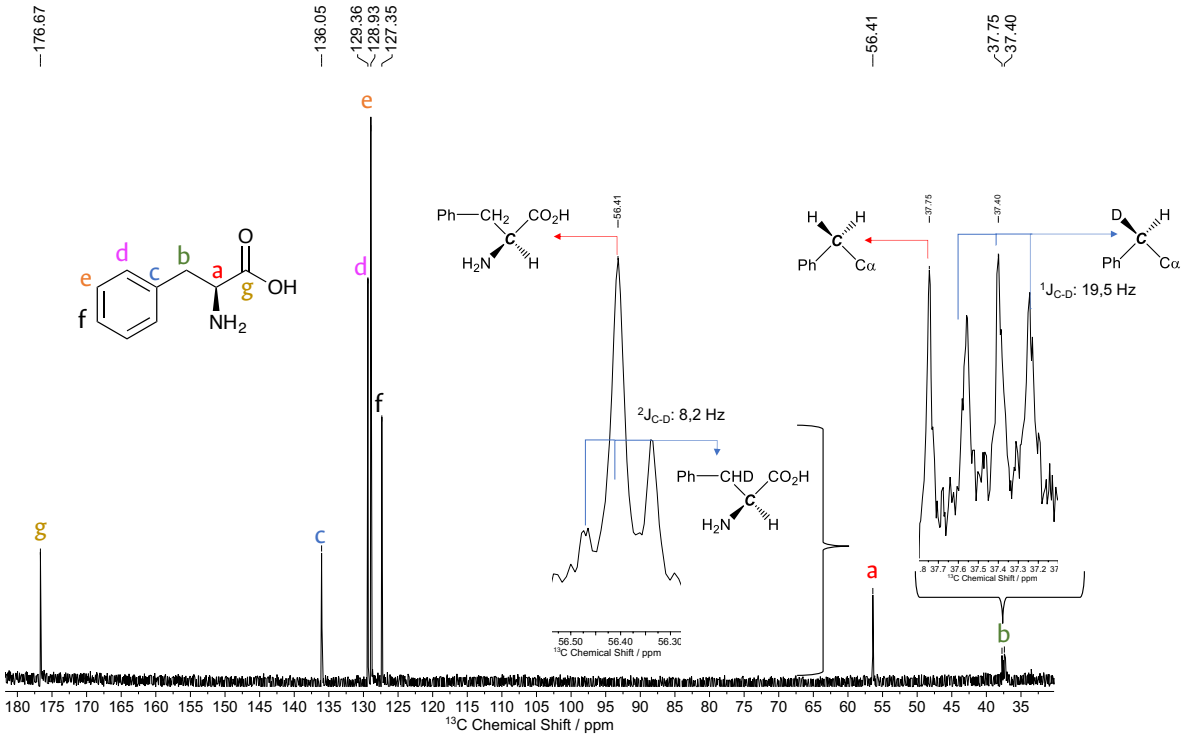

Figure S27. L-phenylalanine deuteration ^{13}C NMR spectrum using **$Pd_{50}Ni_{50}$@IMesPrSO$_3$** (48 h, 55 ºC, 2 bar D_2, 4 mol % metal) (Table 1, Entry 3).

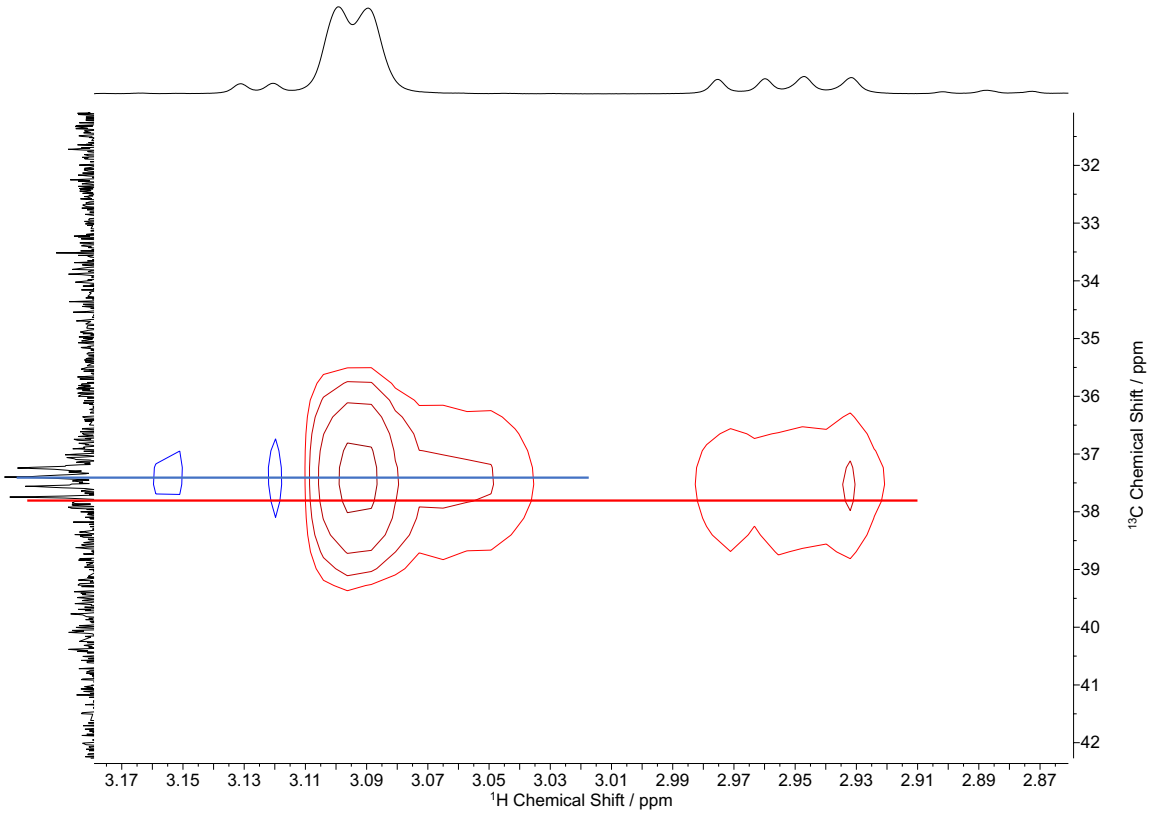

Figure S28. ^{1}H–^{13}C HSQC-NMR spectrum for L-phenylalanine deuteration using **$Pd_{50}Ni_{50}$@IMesPrSO$_3$** (48 h, 55 ºC, 2 bar D_2, 4 mol % metal) (Table 1, Entry 3).

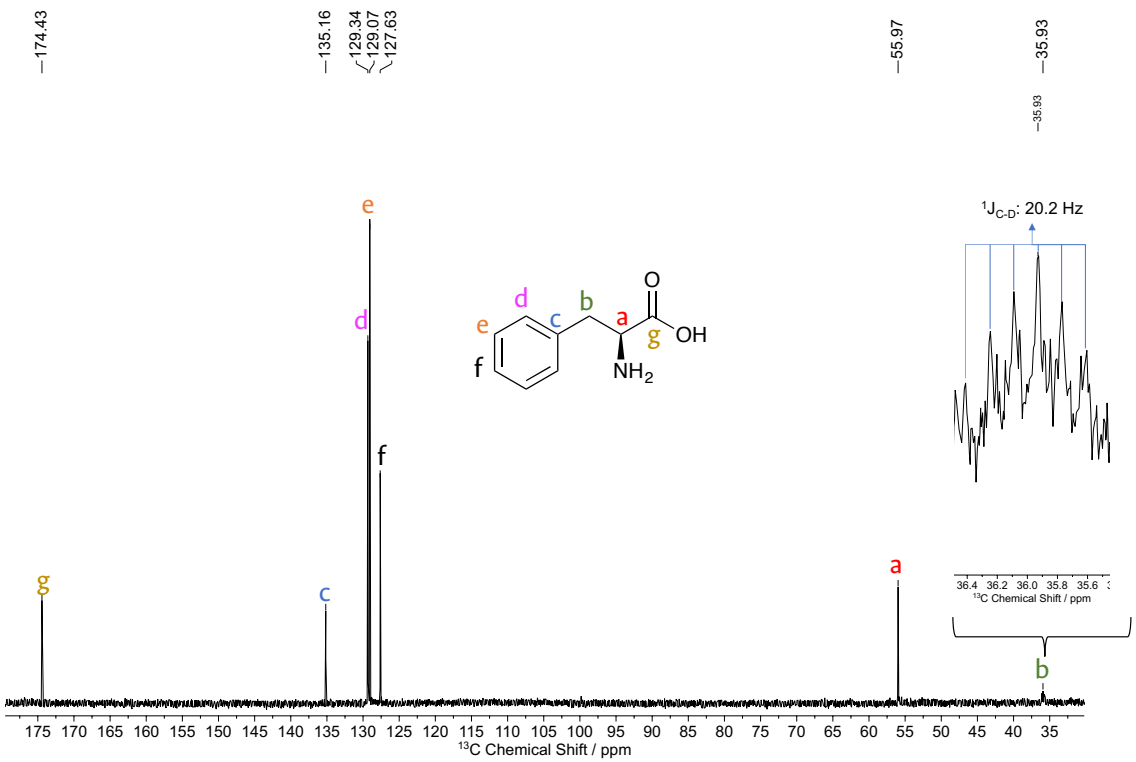

Figure S29. L-phenylalanine deuteration ^{13}C NMR spectrum using **$Pd_{70}Ni_{30}$@IMesPrSO$_3$** (48 h, 55 ºC, 2 bar D_2, 4 mol % metal) (Table 1, Entry 2).

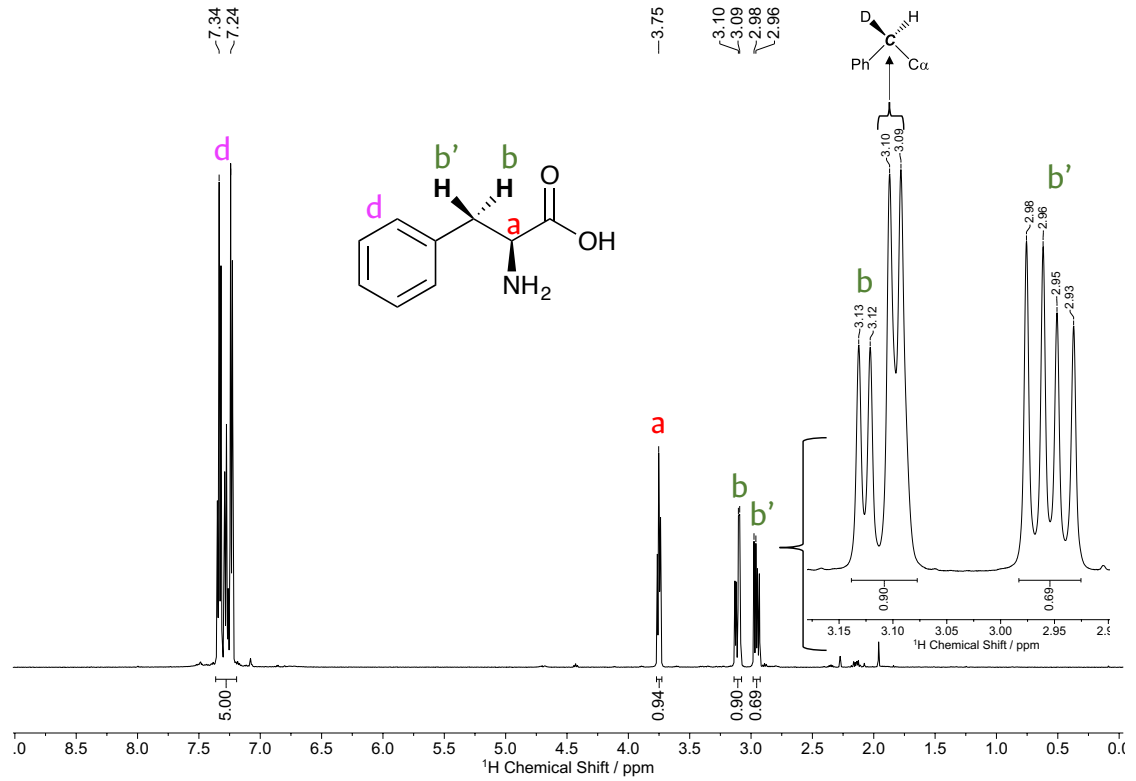

Figure S30. L-phenylalanine deuteration ^{1}H NMR spectrum using **$Pd_{50}Ni_{50}$@IMesPrSO$_3$** (16 h, 55 ºC, 2 bar D_2, 4 mol % metal) (Table 1, Entry 6).

In order to study the enantiospecificity of the first H/D exchange at the CH_2-β position, we recorded the ^{13}C and HSQC experiment on the sample obtained from the catalytic study carried out with **$Pd_{50}Ni_{50}$@IMesPrSO$_3$** in which the deuteration has not been completed (Table 1, Entry 3). In the ^{13}C spectrum (Figure S27) we observed for the C-β a singlet corresponding to the non-deuterated substrate and a triplet with a $^1J_{C\text{-}D}$ = 19.5 Hz assigned to the monodeuterated product. The septuplet expected for the CD_2 product was not observed due to its low intensity. However, this signal was observed in the ^{13}C spectrum for the fully deuterated product (Table 1, Entry 2, Figure S29). In the HSQC experiment (Figure S28), we observed only one cross-peak for the CHD carbon indicating that one monodeuterated diastereoisomer was exclusively formed. According to the literature, it was assigned to (*2S, 3R*)-3-(^{2}H)-phenylalanine.[11] An additional experiment using **$Pd_{50}Ni_{50}$@IMesPrSO$_3$** as a nanocatalyst during 16 h of reaction revealed that a lower deuteration values the same monodeuterated diastereoisomer was formed (Table 1, Entry 6, Figure S30). Thus, the first step of the H/D exchange is enantiospecific with a subsequent second deuteration to yield (*2S*)-3-dideuterium-phenylalanine (Scheme S6). Our results suggest that the first H/D exchange is much faster on one enantiotopic position than the other (diastereoisomer *2S*, *3S* was never observed). Surprisingly, in bimetallic systems, the second H/D exchange on the *2S*, *3R* diastereoisomer is of similar rate than the first step (Table 1, Entries 3, 4 and 6). Additionally, when palladium content is increased, the reaction rate of both steps is improved providing high deuterium incorporation (Table 1, Entry 2).

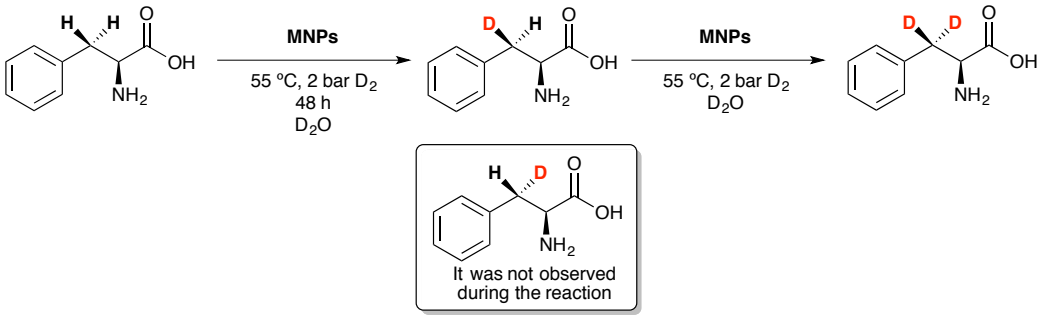

Scheme S6. Enantiospecific H/D exchange at the CH_2-β position in phenylalanine catalyzed by PdNi NPs.

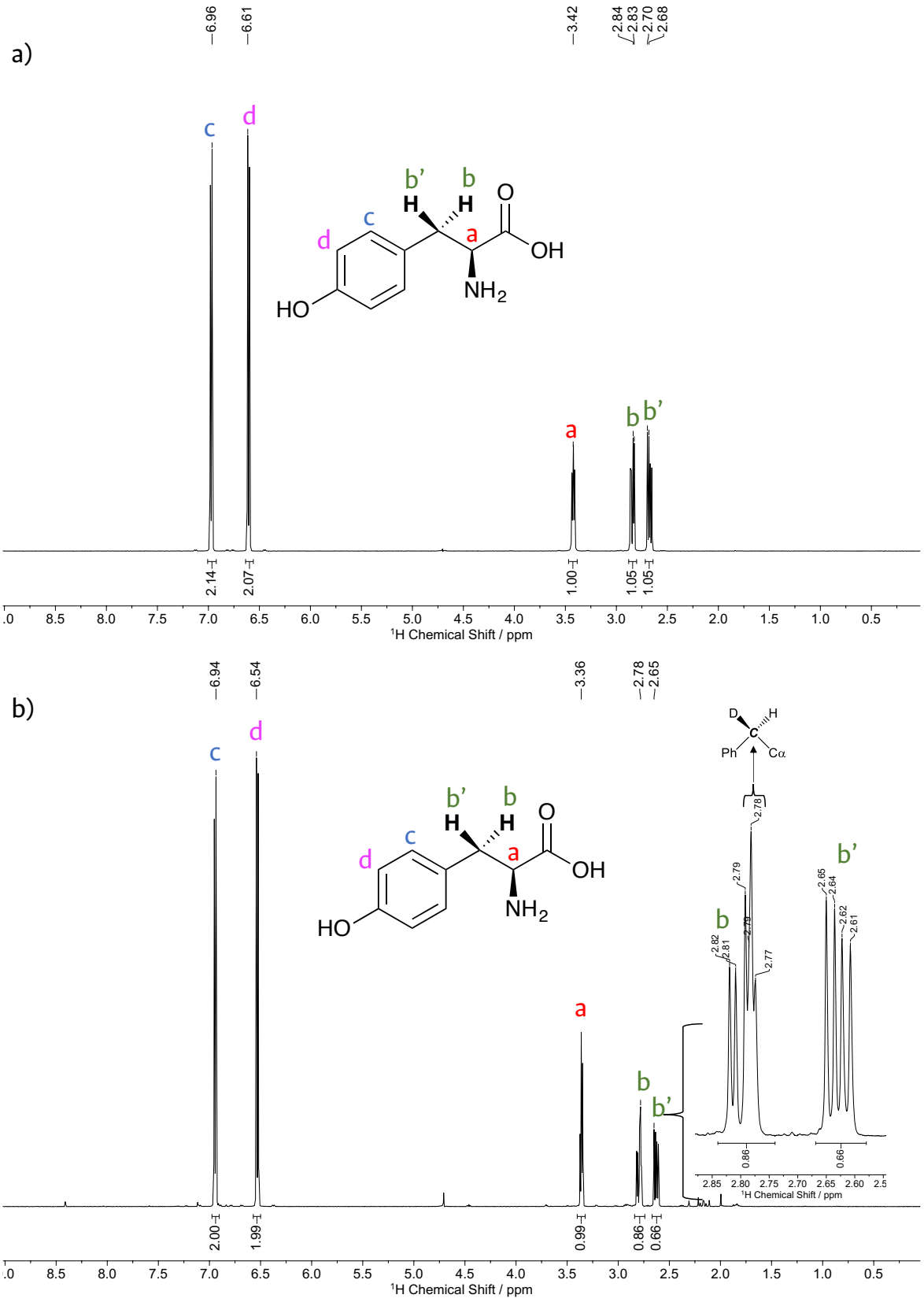

Figure S31. a) L-tyrosine ^{1}H NMR spectrum before deuteration, b) L-tyrosine deuteration using **$Pd_{30}Ni_{70}$@IMesPrSO$_3$** (48 h, 55 ºC, 2 bar D_2, 4 mol % metal) (Table S5, Entry 1).

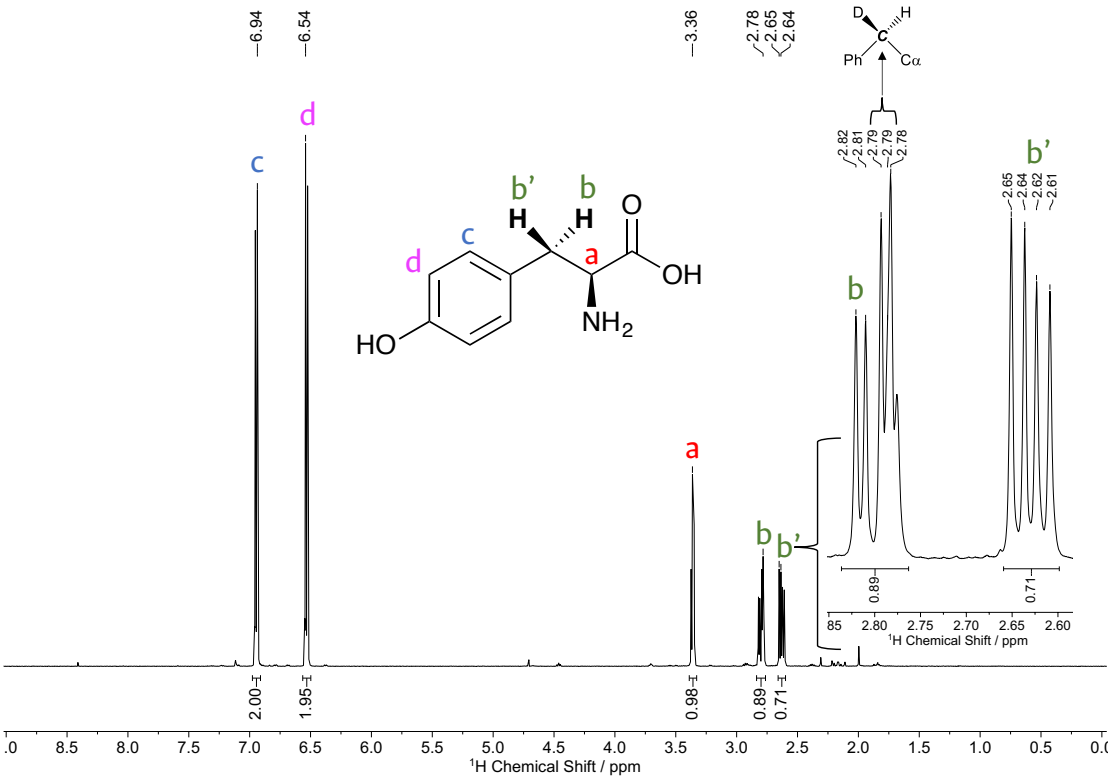

Figure S32. L-tyrosine deuteration using **$Pd_{50}Ni_{50}$@IMesPrSO$_3$** (48 h, 55 ºC, 2 bar D_2, 4 mol % metal) (Table S5, Entry 2).

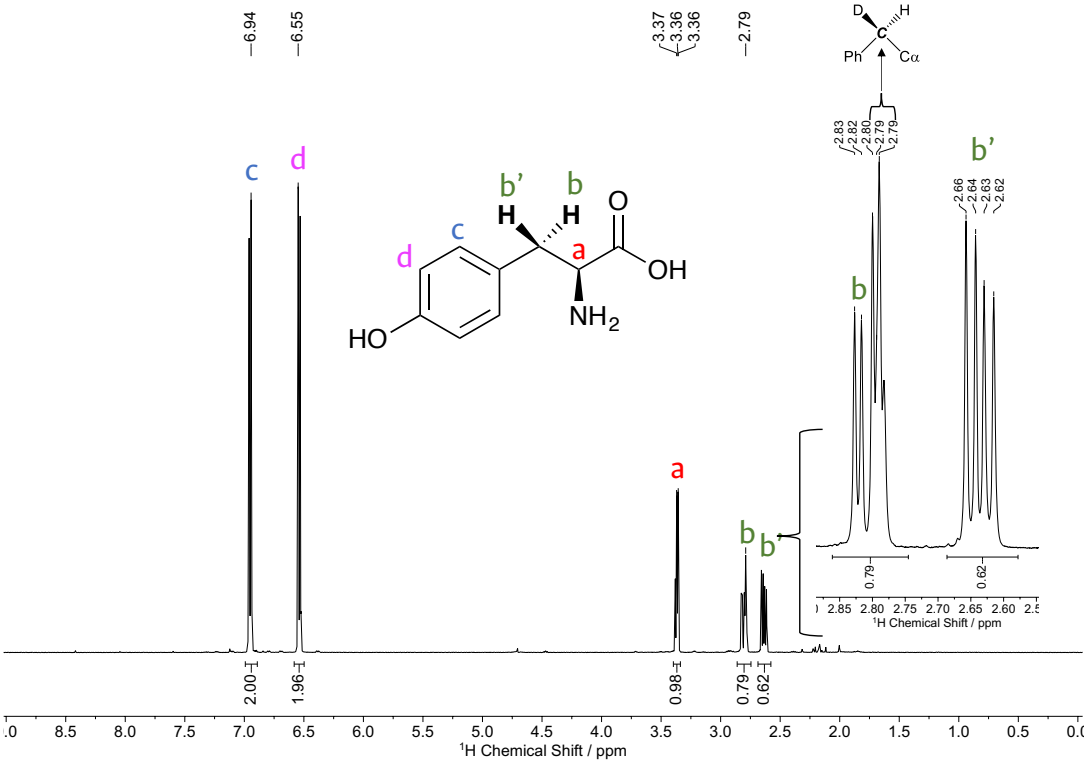

Figure S33. L-tyrosine deuteration using **$Pd_{70}Ni_{30}$@IMesPrSO$_3$** (48 h, 55 ºC, 2 bar D_2, 4 mol % metal) (Table S5, Entry 3).

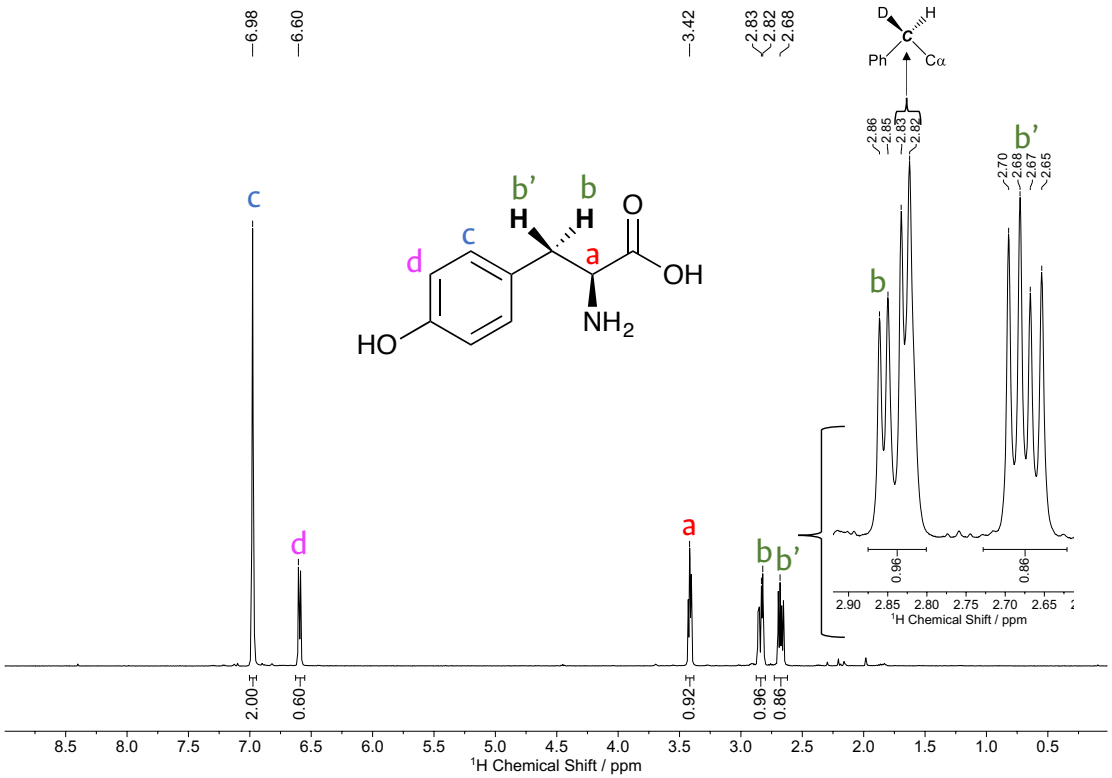

Figure S34. L-tyrosine deuteration using **$Pd_{70}Ni_{30}$@IMesPrSO₃** (48 h, 120 ºC, 2 bar D_2, 4 mol % metal) (Table S5, Entry 4).

Table S5. HIE reaction with L-tyrosine using MNPs as nanocatalysts.[a]

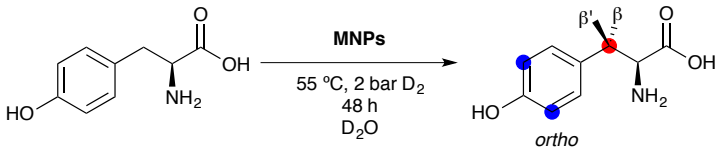

Entry	MNPs	Deuterium incorporation (%)[b]			
		CHD (β')	CD_2 (β'+β)	Total	*ortho*
1	**$Pd_{30}Ni_{70}$@IMesPrSO₃**	10.0	14.0	24.0	-
2	**$Pd_{50}Ni_{50}$@IMesPrSO₃**	9.0	11.0	20.0	-
3	**$Pd_{70}Ni_{30}$@IMesPrSO₃**	8.5	21.0	29.5	-
4[c]	**$Pd_{70}Ni_{30}$@IMesPrSO₃**	5.0	4.0	9.0	70.0

[a] Reaction conditions: 2 bar D_2 (8.1 mmol, 58 eq.), 55 °C, 48h, 4 mol% catalyst (**PdNi@IMesPrSO₃**), 0.1399 mmol of substrate, 2 mL of D_2O and pH=11-12. [b] Determined by ^{1}H NMR. [c] Reaction carried out at 120 °C.

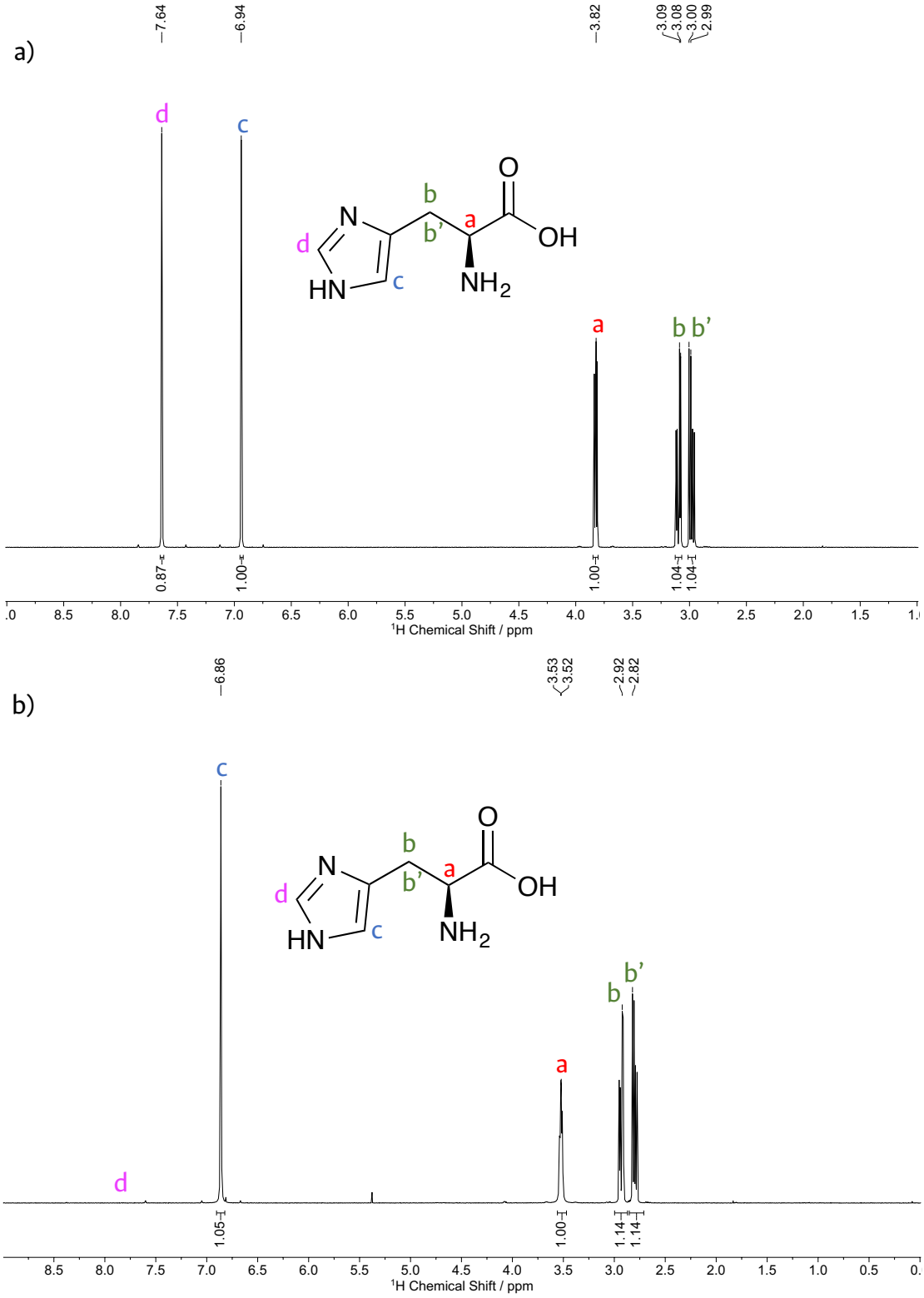

Figure S35. a) L-histidine ^{1}H NMR spectrum before deuteration, b) L-histidine deuteration without catalyst (48 h, 55 ºC, 2 bar D_2) (Table S3, Entry 1).

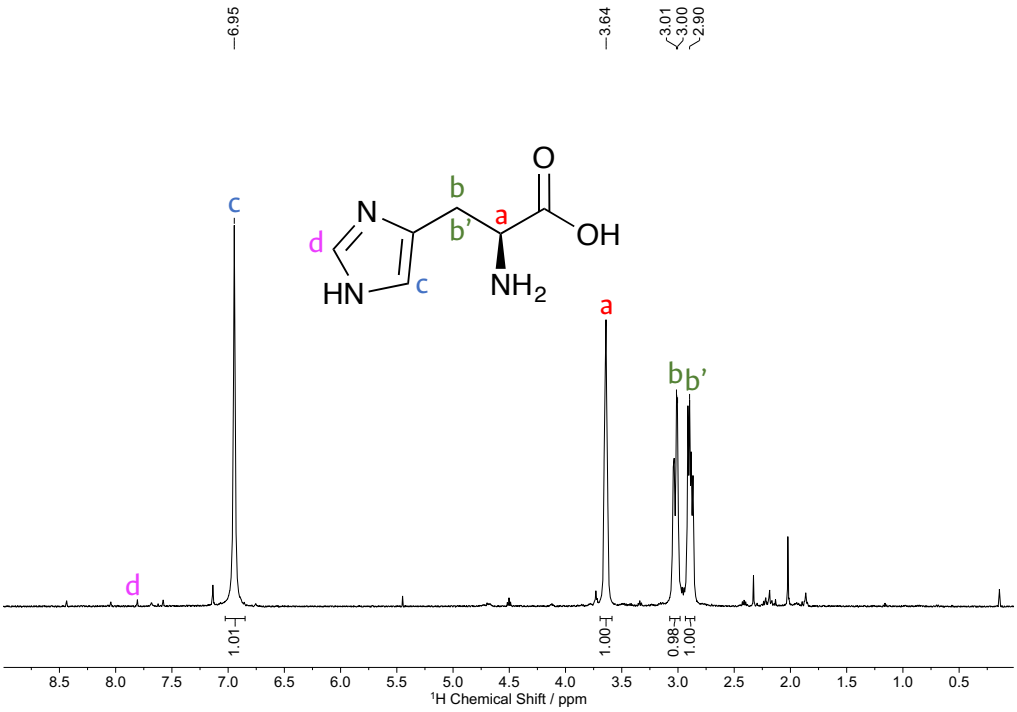

Figure S36. L-histidine deuteration using **Ni@IMesPrSO$_3$** (48 h, 55 ºC, 2 bar D_2, 5 mol % Pd) (Table S3, Entry 2).

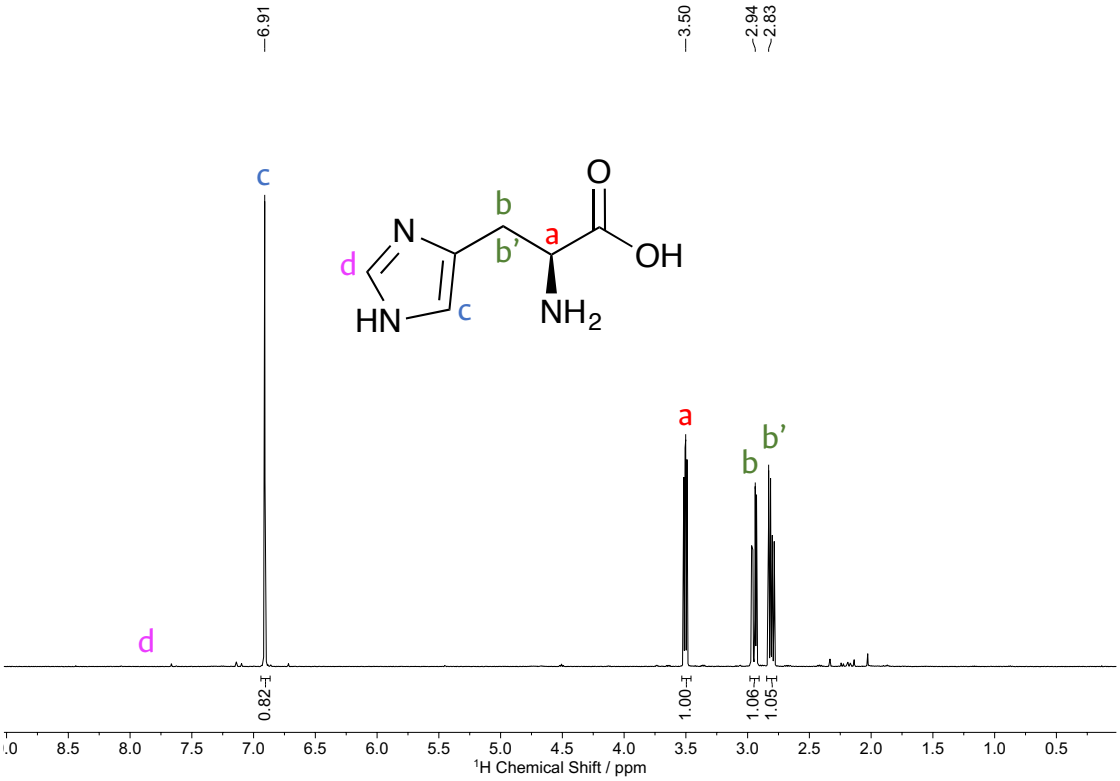

Figure S37. L-histidine deuteration using **Pd@IMesPrSO$_3$** (48 h, 55 ºC, 2 bar D_2, 5 mol % Pd) (Table S3, Entry 3).

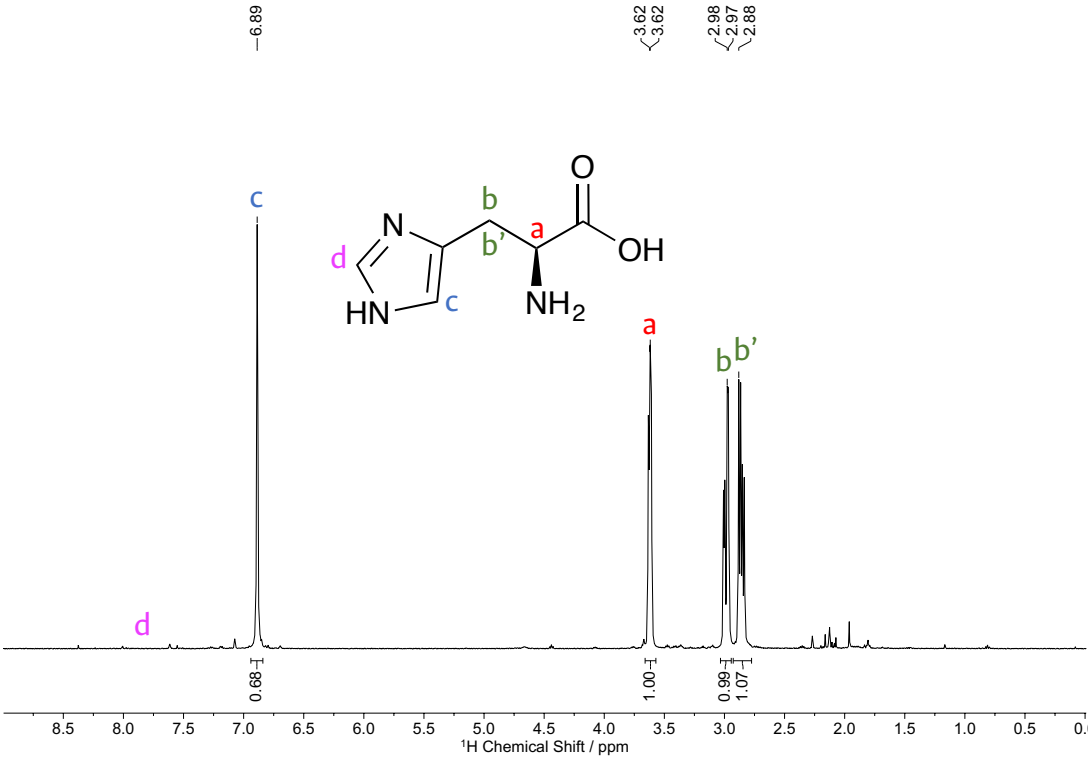

Figure S38. L-histidine deuteration using **$Pd_{70}Ni_{30}$@IMesPrSO$_3$** (48 h, 55 ºC, 2 bar D_2, 4 mol % metal) (Table S3, Entry 4).

Table S6. HIE reaction with L-histidine using MNPs as nanocatalysts.[a]

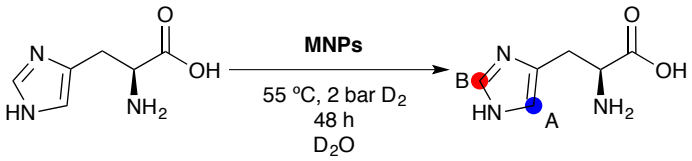

Entry	MNPs	Deuterium incorporation (%)[b]	
		A	B
1	**No nanocatalyst**	-	99.0
2	**Ni@IMesPrSO$_3$**	-	99.0
3	**Pd@IMesPrSO$_3$**	18.0	99.0
4	**$Pd_{70}Ni_{30}$@IMesPrSO$_3$**	32.0	99.0

[a] Reaction conditions: 2 bar D_2 (8.1 mmol, 58 eq.), 4 mol% catalyst (**PdNi@IMesPrSO$_3$**), 5 mol% (**Pd@IMesPrSO$_3$**, **Ni@IMesPrSO$_3$**), 0.1399 mmol of substrate, 2 mL of D_2O and pH=8-9. [b] Determined by ^{1}H NMR.

13. References

(1) Scofield, J. H. *Theoretical Photoionization Cross Sections from 1 to 1500 KeV.*; U.S. Atomic Energy Commission, 1973. https://doi.org/10.2172/4545040.

(2) Moore, L. R.; Cooks, S. M.; Anderson, M. S.; Schanz, H.-J.; Griffin, S. T.; Rogers, R. D.; Kirk, M. C.; Shaughnessy, K. H. Synthesis and Characterization of Water-Soluble Silver and Palladium Imidazol-

2-Ylidene Complexes with Noncoordinating Anionic Substituents. *Organometallics* **2006**, *25* (21), 5151–5158. https://doi.org/10.1021/om060552b.

(3) Amiens, C.; Chaudret, B.; Ciuculescu-Pradines, D.; Collière, V.; Fajerwerg, K.; Fau, P.; Kahn, M.; Maisonnat, A.; Soulantica, K.; Philippot, K. Organometallic Approach for the Synthesis of Nanostructures. *New J. Chem.* **2013**, *37* (11), 3374. https://doi.org/10.1039/c3nj00650f.

(4) Martínez-Prieto, L. M.; Baquero, E. A.; Pieters, G.; Flores, J. C.; De Jesús, E.; Nayral, C.; Delpech, F.; Van Leeuwen, P. W. N. M.; Lippens, G.; Chaudret, B. Monitoring of Nanoparticle Reactivity in Solution: Interaction of l-Lysine and Ru Nanoparticles Probed by Chemical Shift Perturbation Parallels Regioselective H/D Exchange. *Chem. Commun.* **2017**, *53* (43), 5850–5853. https://doi.org/10.1039/c7cc02445b.

(5) Martínez-Prieto, L. M.; Cano, I.; Márquez, A.; Baquero, E. A.; Tricard, S.; Cusinato, L.; del Rosal, I.; Poteau, R.; Coppel, Y.; Philippot, K.; Chaudret, B.; Cámpora, J.; van Leeuwen, P. W. N. M. Zwitterionic Amidinates as Effective Ligands for Platinum Nanoparticle Hydrogenation Catalysts. *Chem. Sci.* **2017**, *8* (4), 2931–2941. https://doi.org/10.1039/C6SC05551F.

(6) Baquero, E. A.; Tricard, S.; Flores, J. C.; de Jesús, E.; Chaudret, B. Highly Stable Water-Soluble Platinum Nanoparticles Stabilized by Hydrophilic N-Heterocyclic Carbenes. *Angew. Chemie Int. Ed.* **2014**, *53* (48), 13220–13224. https://doi.org/10.1002/anie.201407758.

(7) Moddeman, W. E.; Bowling, W. C.; Carter, D. C.; Grove, D. R. XPS Surface and Bulk Studies of Heat Treated Palladium in the Presence of Hydrogen at 150°C. *Surf. Interface Anal.* **1988**, *11* (6–7), 317–326. https://doi.org/10.1002/sia.740110609.

(8) Martínez-Prieto, L. M.; Rakers, L.; López-Vinasco, A. M.; Cano, I.; Coppel, Y.; Philippot, K.; Glorius, F.; Chaudret, B.; van Leeuwen, P. W. N. M. Soluble Platinum Nanoparticles Ligated by Long-Chain N-Heterocyclic Carbenes as Catalysts. *Chem. Eur. J.* **2017**, *23* (52), 12779–12786. https://doi.org/10.1002/chem.201702288.

(9) Powell, C. J. Recommended Auger Parameters for 42 Elemental Solids. *J. Electron Spectros. Relat. Phenomena* **2012**, *185* (1–2), 1–3. https://doi.org/10.1016/j.elspec.2011.12.001.

(10) Senō, M.; Tsuchiya, S.; Hidai, M.; Uchida, Y. X-Ray Photoelectron Spectra of Aryl-Nickel Complexes. *Bull. Chem. Soc. Jpn.* **1976**, *49* (5), 1184–1186. https://doi.org/10.1246/bcsj.49.1184.

(11) Barnett, D. W.; Panigot, M. J.; Curley, R. W. Stereoselective Route to 15N-Labeled-β-Deuterated Amino Acids: Synthesis of (2S,3R)-[3-2H,15N]-Phenylalanine. *Tetrahedron: Asymmetry* **2002**, *13* (17), 1893–1900. https://doi.org/10.1016/S0957-4166(02)00487-1.